Ferromagnetic multilayers: Statics and dynamics

D. Schwenk, F. Fishman, and F. Schwabl
Institut für Theoretische Physik, Physik-Department der Technischen Universität München, D-8046 Garching, West Germany
(Received 19 February 1988)

A theory of periodic multilayers consisting of two alternating ferromagnetic materials with different transition temperatures is presented. The theory is based on an inhomogeneous Ginzburg-Landau (GL) functional, where the GL coefficients are chosen to model the alternating layers and interface interactions. The transition temperature of the composite material is derived by use of the linear stability analysis of the inhomogeneous GL functional. The static magnetization profiles for different temperatures are calculated analytically. It is shown that the magnetization penetrating into the low-temperature ferromagnet falls off inversely with distance close to T_1 and exponentially far above T_1, where T_1 is the lower transition temperature. We also consider the average magnetization of this multilayer system and its characteristic temperature dependence. The spin dynamics are studied by use of a generalized Bloch equation. Different limiting cases as well as the general situation with both dipolar and exchange interactions are considered. The magnon dispersion relation is computed and by symmetry considerations, it is shown that the gaps vanish at certain values of the wave vector **k**. The inelastic neutron scattering cross section is calculated. With appropriate modifications the theory can be applied to other systems undergoing phase transitions, such as ferroelectrics.

I. INTRODUCTION

Great technological progress has been achieved recently in growing magnetic superlattices, the parameters of which (e.g., layer thickness and material composition) can be controlled accurately.[1] These magnetic multilayers have potential applications in the construction of microwave devices and can act as frequency filters or delay elements.[2] Another application is neutron optics, where the superlattices serve as monochromators, polarizers,[3] or mirrors,[4] depending on material composition and layer thickness.

Furthermore, there has always been great interest in the study of such artificial structures, whose properties can differ drastically from the bulk ones. A variety of cases, depending upon the nature of the constituents, have been studied: ferromagnetic-nonmagnetic layers,[5,6] ferromagnet-antiferromagnet layers,[7,8] and ferromagnet-superconductor layers.[9] A study of the excitations in ferromagnetic multilayers, based on the Heisenberg Hamiltonian, has been performed recently.[10,11] The ferromagnetic resonance spectrum, taking into account only exchange interactions, has been also considered.[12]

Hence, there is a need for a complete theory of the static and dynamical behavior in ferromagnetic superlattices, when both dipolar and exchange interactions are taken into account. In this work we present such a theory based on a continuum approach. A brief account of some aspects of this study has been reported recently.[13] Our theory is based on a Ginzburg-Landau (GL) free-energy functional and the advantage of this phenomenological description is that it is material independent and can be applied equally well to the other multilayer structures undergoing a phase transition, e.g., ferroelectrics. However, to be specific, in most of the figures we use material parameters of EuS and EuO, which are promising candidates for such ferromagnetic superlattices. In the study of static properties of superlattices the following questions are of special interest: (i) what is the transition temperature of this structure; (ii) what is the magnetization profile; (iii) what is the temperature dependence of the average magnetization, and of course, how all these quantities depend on the material parameters of the bulk constituents and superlattice geometry. In our model we incorporate also interface effects, because the magnetic properties of the layers near the interfaces may change as a result of the structural and electronic mismatch of the constituents. In order to characterize these effects we introduce a phenomenological interface energy term into the GL functional and examine its influence on the transition temperature.

A major portion of the work is devoted to the spin wave excitations in these structures. The dynamical part of our theory is based on the generalized stochastic Bloch equation, which has been used successfully in the field of critical dynamics.[14] Because the dominant "superlattice effect" on the magnon spectrum is the appearance of "miniband structure," it is particularly important to understand the following points: (i) what are the contributions of different interactions to the magnon spectrum; (ii) what are Damon-Eshbach modes in multilayers, which were studied previously only in single films (or in the system of ferromagnetic films separated by a nonmagnetic material);[5,15] (iii) how the symmetry of the pure exchange interaction influences the magnon spectrum and what predictions about the gaps can be made in this limit; (iv) what predictions about minibands and minigaps can be made solely from the knowledge of the bulk magnon dispersion relations of the layer constituents.

Because neutron scattering experiments are important

techniques to probe the magnon spectrum, we also calculate the inelastic neutron scattering cross section for our multilayer system.

The outline of this paper is as follows. In Sec. II we describe the model, the GL free-energy functional for inhomogeneous media, and the GL coefficients. In this section we also discuss the GL equation and the boundary conditions obeyed by the static magnetization at the interfaces between the layers. Section III contains the calculation of the transition temperature of the layer system, the magnetization profiles for different temperatures, as well as the temperature dependence of the total magnetization. In Sec. IV we consider the dynamics of our system. First we discuss the limiting cases of pure dipolar and pure exchange interactions. In the dipolar case we discuss the properties of the Damon-Eshbach modes. The magnon spectrum for the pure exchange case contains gaps, which vanish at certain values of the wave vector $\mathbf{k}$. We present symmetry considerations leading to this phenomenon. After these two limiting cases, we turn our attention to the general case, where both dipolar and exchange interactions are included. We discuss again the possibility of the vanishing of gaps and compare the results with pure dipolar and exchange cases. In Sec. V we consider the inelastic neutron scattering cross section and show how the vanishing of gaps in the magnon spectrum leads to an increase in the cross section. In Sec. VI we present a summary of the results. In Appendix A we discuss alternative formulations of the free-energy GL functional of the layer system. Appendix B contains some results concerning the "δ model," which can be applied for ultrathin layers. The details of the numerical procedure can be found in Appendix C.

II. THE MODEL

Now, we introduce the basic constituents of our model. We consider a composite material made of two periodically arranged isotropic ferromagnetic layers. The geometry is shown in Fig. 1. The layer planes define the y-z plane and the thicknesses of the layers are denoted by D_1 and D_2. Our treatment will be based on the Ginzburg-Landau theory, hence we start with a discussion of the form of the GL free-energy functional of the composite material.

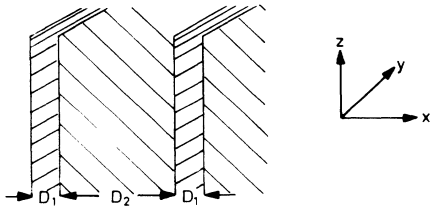

FIG. 1. Geometry of the periodic layer structure. Thicknesses of layers 1 and 2 are D_1 and D_2.

A. Free-energy functional

The composite ferromagnetic material is characterized by the local magnetization $\mathbf{M}(\mathbf{x})$. The probability distribution for $\mathbf{M}(\mathbf{x})$ is given by $\exp(-F[\mathbf{M}]/kT)$ up to normalization, where the GL free-energy functional $F[\mathbf{M}]$ of our inhomogeneous material has the form[16,17]

$$F[\mathbf{M}]=\tfrac{1}{2}\int d^3x\,\Big[a(\mathbf{x})\mathbf{M}^2+\tfrac{1}{2}b(\mathbf{x})(\mathbf{M}^2)^2 +c(\mathbf{x})\sum_i(\nabla M_i)^2-\mathbf{M}\mathbf{H}^m-2\mathbf{M}\mathbf{H}\Big]. \tag{2.1}$$

Here $\mathbf{H}$ and $\mathbf{H}^m$ are the external and demagnetization fields. The order parameter $\mathbf{M}(\mathbf{x})$ and the GL coefficients $a(\mathbf{x})$, $b(\mathbf{x})$, and $c(\mathbf{x})$ are defined throughout the whole sample and are continuous functions of $\mathbf{x}$. Far from the interfaces these parameters reach their bulk values, but change rapidly in the transition region between layers. In Fig. 2 we show the typical forms, which $a(\mathbf{x})$ can have for periodically arranged multilayer structures. The forms of $a(\mathbf{x})$ with drastic increase (decrease) near the interfaces, account for the possibility of a reduced (enhanced) tendency for order in these regions. The bulk GL parameters of material 1 and 2 we denote by a_α, b_α, and c_α, with $\alpha=1,2$. As usual, the temperature dependence is attributed to $a_\alpha(T)$ only, namely $a_\alpha(T)=a'_\alpha(T-T_\alpha)$, where T_1 and T_2 are the bulk Curie temperatures of the two materials. Without loss of generality we assume $T_2>T_1$. Because we consider isotropic materials, the free energy (2.1) does not contain anisotropy terms. It would pose no principal difficulty to include these terms or to allow for a more complicated temperature dependence of the GL parameters. However, the main qualitatively important features result already from the difference in the transition temperatures.

For long-wavelength properties the continuous $a(\mathbf{x})$, as represented in Fig. 2, can be replaced by the following discontinuous form:

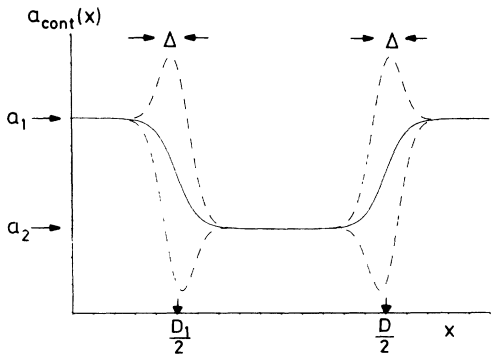

FIG. 2. Possible shape of the continuously varying GL parameter $a_{\rm cont}(x)$. Dashed line corresponds to $a_s>0$ and dash-dotted line to $a_s<0$.

$$a(\mathbf{x})=\sum_{n=-\infty}^{\infty}\sum_{\alpha=1,2}a_\alpha\Theta\left[\tfrac{1}{2}D_\alpha-\left|x-\left[n+\frac{\alpha-1}{2}\right]D\right|\right]+\sum_{n=-\infty}^{\infty}a_s\delta\left[\frac{D_1}{2}-|x-nD|\right], \tag{2.2a}$$

with $a_s=\int_{-\Delta/2}^{\Delta/2}a_{\rm cont}(x+D_1/2)dx$. Here $D=D_1+D_2$ is the lattice constant of the superlattice. $\Theta(y)$ and $\delta(y)$ are usual step and δ functions, and Δ is the width of the transition region. By $a_{\rm cont}(\mathbf{x})$ we denoted the continuous $a(\mathbf{x})$ as represented in Fig. 2. Later we will show that this approximation is valid when the transition region Δ is narrow, namely $\Delta\ll\xi_\alpha$, where $\xi_\alpha(T)=\sqrt{(c_\alpha/|a_\alpha(T)|)}$ are the coherence lengths. This discontinuous form of $a(\mathbf{x})$ together with similar expressions for $b(\mathbf{x})$ and $c(\mathbf{x})$,

$$b(\mathbf{x})=\sum_{n=-\infty}^{\infty}\sum_{\alpha=1,2}b_\alpha\Theta\left[\tfrac{1}{2}D_\alpha-\left|x-\left[n+\frac{\alpha-1}{2}\right]D\right|\right], \tag{2.2b}$$

$$c(\mathbf{x})=\sum_{n=-\infty}^{\infty}\sum_{\alpha=1,2}c_\alpha\Theta\left[\tfrac{1}{2}D_\alpha-\left|x-\left[n+\frac{\alpha-1}{2}\right]D\right|\right], \tag{2.2c}$$

In some multilayer structures made of isotropic ferromagnetic materials, the interface introduces a strong anisotropic behavior. Such effects can be accounted for by adding to the free-energy density, Eq. (2.1), an additional term of the form

$$f_{\rm an}[\mathbf{M}(\mathbf{x})]=K\sum_n\delta\left[\frac{D_1}{2}-|x-nD|\right](\mathbf{n}\cdot\mathbf{M})^2, \tag{2.3}$$

where $\mathbf{n}$ is a unit vector normal to the interface.

To conclude the discussion of the free-energy functional of the multilayer structure, we want to point out that there exists another slightly different approach to define the free energy of the composite material. We refer the reader to the Appendix A, where this approach is discussed.

B. Ginzburg-Landau equation and the boundary conditions

To obtain the gross features of our system we may limit ourselves to the Gaussian approximation, which is valid except in the immediate vicinity of the critical point. This implies that the magnetization is given by the most probable configuration, which is determined by $\delta F/\delta\mathbf{M}=0$. Using the free-energy functional (2.1), we obtain

$$[a(\mathbf{x})+b(\mathbf{x})\mathbf{M}_0^2-\partial_i c(\mathbf{x})\partial_i]\mathbf{M}_0=\mathbf{H}_0^m+\mathbf{H}. \tag{2.4}$$

The demagnetization field $\mathbf{H}_0^m$ obeys the quasistatic Maxwell's equations

$$\mathrm{rot}\mathbf{H}_0^m=0, \tag{2.5a}$$

$$\mathrm{div}(\mathbf{H}_0^m+4\pi\mathbf{M}_0)=0. \tag{2.5b}$$

The solution of Eqs. (2.4) and (2.5) describes the magnetization profile throughout the whole sample. The real GL coefficients $a(\mathbf{x})$, $b(\mathbf{x})$, and $c(\mathbf{x})$ are continuous, thus Eq. (2.4) implies the continuity of $\mathbf{M}_0(\mathbf{x})$ and its derivatives. If, on the other hand, for mathematical convenience the discontinuous idealizations Eqs. (2.2a) to (2.2c) are used and the equations are solved within individual layers, these elements have to be joined by boundary conditions.

Because the GL parameters (2.2) depend only on x, Eq. (2.4) is an ordinary second-order differential equation and only the boundary conditions on $\mathbf{M}_0(\mathbf{x})$ and $\partial_x\mathbf{M}_0$ are needed. In the following we put $\mathbf{H}=0$ and assume $\mathbf{H}_0^m=0$ and $\mathbf{M}_0=M_0(x)\hat{\mathbf{e}}_z$, which will be shown below for the geometry of the interest. Because the most singular term in the GL coefficients (2.2) is a δ function, $M_0(x)$ has to be continuous. Furthermore, integrating Eq. (2.4) from $-\varepsilon$ to $\varepsilon(\varepsilon\to0)$ around the interface located at $x=D_1/2$, we get

$$\lim_{\varepsilon\to0}[c(x)\partial_x M_0(x)]\Big|_{(D_1/2)-\varepsilon}^{(D_1/2)+\varepsilon}=\lim_{\varepsilon\to0}\int_{(D_1/2)-\varepsilon}^{(D_1/2)+\varepsilon}[a(x)+b(x)M_0^2]M_0(x)dx. \tag{2.6}$$

Inserting Eqs. (2.2) and keeping in mind that $M_0(x)$ is continuous, Eq. (2.6) reduces to

$$c_2\partial_x M_{02}-c_1\partial_x M_{01}=a_s M_0\left[\frac{D_1}{2}\right]. \tag{2.7}$$

Here $\partial_x M_{02}$ ($\partial_x M_{01}$) denote the derivatives of the magnetization just right (left) of the interface. Equation (2.7) together with the continuity of M_0, i.e., $M_{01}=M_{02}$, constitute the boundary conditions following from Eq. (2.4) for the discontinuous GL coefficients (2.2a) and (2.2b).

We are now in a position to discuss precisely the condition under which it is allowed to replace GL coefficients which originally were smooth by their discontinuous counterparts. Also, it is worth noting that at first sight, the condition (2.7) contradicts the previously discussed continuity of $\partial_x M_0(x)$. To elucidate this point, let us consider GL coefficients to be continuous, e.g., $a(x)$ to be as shown in Fig. 2, and integrate Eq. (2.4) from $(D_1-\Delta)/2$ to $(D_1+\Delta)/2$. We obtain

$$c_{\rm cont}\left[\frac{D_1}{2}+\frac{\Delta}{2}\right]\partial_x M_0\left[\frac{D_1}{2}+\frac{\Delta}{2}\right]-c_{\rm cont}\left[\frac{D_1}{2}-\frac{\Delta}{2}\right]\partial_x M\left[\frac{D_1}{2}-\frac{\Delta}{2}\right]=\int_{(D_1-\Delta)/2}^{(D_1+\Delta)/2}[a_{\rm cont}(x)+b_{\rm cont}(x)M_0^2]M_0(x)dx. \tag{2.8}$$

We will show later that $M_0(x)$ changes on the scale of ξ_α. Hence, near the interface $\partial_x M_0\sim M_0(D_1/2)/\xi_\alpha$ and

$$M_0(x)\simeq M_0(D_1/2)[1+(D_1/2+x)/\xi_\alpha] .$$

Substituting this into (2.8), we get

$$c_{\rm cont}\left[\frac{D_1}{2}+\frac{\Delta}{2}\right]\partial_x M_0\left[\frac{D_1}{2}+\frac{\Delta}{2}\right]-c_{\rm cont}\left[\frac{D_1}{2}-\frac{\Delta}{2}\right]\partial_x M_0\left[\frac{D_1}{2}-\frac{\Delta}{2}\right]$$
$$\simeq M_0\left[\frac{D_1}{2}\right]\int_{(D_1-\Delta)/2}^{(D_1+\Delta)/2} a_{\rm cont}(x)dx+M_0^3\left[\frac{D_1}{2}\right]\int_{(D_1-\Delta)/2}^{(D_1+\Delta)/2} b_{\rm cont}(x)dx+0\left[\frac{\Delta}{\xi_\alpha}\right] . \quad (2.9)$$

The first term on the right-hand side is just $M_0(D_1/2)a_s$, with the definition of a_s given in (2.2a). For the smooth $b_{\rm cont}(x)$ and narrow transition region Δ, the second term is of order $M_0^3(D_1/2)b_{\rm cont}(D_1/2)\Delta$. Hence, for narrow transition regions $[\Delta/\xi_\alpha\to 0$ and $M_0^3 b_{\rm cont}(D_1/2)\Delta\to 0]$ the right-hand side of (2.9) reduces to $M_0(D_1/2)a_s$, and $c_{\rm cont}[(D_1+\Delta)/2]$ and $c_{\rm cont}[(D_1-\Delta)/2]$ reduce to c_2 and c_1, correspondingly. The comparison of (2.7) and (2.9) explains also the meaning of $\partial_x M_{01}$ and $\partial_x M_{02}$, which in the case of continuous GL parameters are just the derivatives at the "borders" of the transition region. In this sense Eq. (2.7) should be understood. We also see that the discontinuous approximation for GL parameters is valid when $\Delta/\xi_\alpha \ll 1$. We will assume throughout this paper that this condition is fulfilled and we will use the boundary condition (2.7).

Finally, the demagnetization field $\mathbf{H}_0^m$ satisfies the usual electromagnetic boundary conditions, namely that the component of $\mathbf{H}_0^m$ parallel to the surface and the component of $\mathbf{B}=\mathbf{H}_0^m+4\pi\mathbf{M}_0$ normal to it are continuous.

III. TRANSITION TEMPERATURE AND MAGNETIZATION

Now we suppose that the composite material has the form of a slab with dimensions $L_y, L_z \gg L_x$ and set $\mathbf{H}=0$. To find the equilibrium magnetization $\mathbf{M}_0(x)$, we have to solve Eqs. (2.4) and (2.5). Keeping in mind that $\mathbf{M}_0$ depends only on x, we note that Maxwell's equations (2.5) are solved by $\mathbf{H}_0^m=(-4\pi M_{0x},0,0)$. This solution for $\mathbf{H}_0^m$ is correct in the limit L_x/L_z and $L_x/L_y\to 0$, and it obviously satisfies the electromagnetic boundary conditions on the interfaces.[18]

Therefore, the term $-\mathbf{H}_0^m\mathbf{M}_0$ in the free energy (2.1)—and the free energy itself—are minimal for $\mathbf{M}_0$ parallel to the layers; e.g., $\mathbf{M}_0(x)=M_0(x)\hat{\mathbf{e}}_z$. The static demagnetization field is zero in this geometry. This justifies the assumptions $\mathbf{H}_0^m=0$ and $\mathbf{M}_0\|\hat{\mathbf{z}}$ made above in the derivation of the boundary conditions.

A. Transition temperature

It is obvious that $\mathbf{M}_0=0$ for $T>T_2$. In the temperature region $T_1<T<T_2$ the system undergoes a second-order phase transition at some temperature T_c, below which the magnetization is nonzero. We could find T_c by solving Eq. (2.4) and investigating in what temperature region its nonzero solution minimizes the free-energy functional (2.1).

However, instead we will use an alternative method and find T_c directly from the stability limit of the free-energy functional (2.1) against harmonic fluctuations around zero magnetization, $M_0=0$.[19] The harmonic fluctuations following from the free-energy functional (2.1) are determined in the paramagnetic phase by the linear operator

$$L=-\frac{\partial}{\partial x}c(x)\frac{\partial}{\partial x}+a(x) , \quad (3.1a)$$

the orthonormal eigenfunctions of which are denoted by $M_\lambda(x)$; i.e.,

$$LM_\lambda(x)=\varepsilon_\lambda M_\lambda(x) . \quad (3.1b)$$

If we expand $M(x)$ in terms of $M_\lambda(x)$; i.e.,

$$M_0(x)=\sum_\lambda B_\lambda M_\lambda(x) ,$$

with coefficients B_λ, the free-energy functional is given in second order by

$$F=\tfrac{1}{2}\sum_\lambda \varepsilon_\lambda |B_\lambda|^2 . \quad (3.1c)$$

If all $\varepsilon_\lambda>0$, then $F>0$ and the minimum of F is reached for $M_0=0$. But if at least one $\varepsilon_{\lambda_0}<0$, the uniform solution is unstable. Then one has to go beyond the harmonic approximation. Immediately below the instability point one finds for the minimum of the free-energy functional, $M_0(x)\simeq M_{\lambda_0}(x)$. Therefore, the transition temperature T_c is defined by the condition that the lowest eigenvalue ε_{λ_0} is zero.

Noting that for $T_1<T<T_2$, $a_2(T)<0$ and $a_1(T)>0$ we can easily solve Eq. (3.1b). The solution of this equation with $\varepsilon_{\lambda_0}=0$ is

$$M_{\lambda_0}(x)=\begin{cases}\cos\left[\dfrac{D_2}{2\xi_2}\right]\dfrac{\cosh(x/\xi_1)}{\cosh(D_1/2\xi_1)} & \text{for } |x|\le\dfrac{D_1}{2} ,\\ \cos\left[\dfrac{x-D/2}{\xi_2}\right] & \text{for } \left|x-\dfrac{D}{2}\right|<\dfrac{D_2}{2} .\end{cases} \quad (3.2a)$$

This solution has to satisfy the boundary conditions (2.7) and this gives the implicit equation for T_c

$$\frac{c_1}{\xi_1(T_c)}\tanh\left[\frac{D_1}{2\xi_1(T_c)}\right] = \frac{c_2}{\xi_2(T_c)}\tan\left[\frac{D_2}{2\xi_2(T_c)}\right] - a_s \ . \quad (3.2b)$$

Equation (3.2b) is valid only for

$$a_s \geq a_s^c \equiv -\frac{c_1}{\xi_1(T_2)}\tanh\frac{D_1}{2\xi_1(T_2)} \ . \quad (3.2c)$$

The transition temperature T_c lies in the temperature interval

$$T_{\min} \equiv T_2\left[1-\frac{\pi^2\xi_2^2(0)}{D_2^2}\right] \leq T_c \leq T_2 \ , \quad (3.3)$$

as can be readily seen from the graphical solution of Eq. (3.2b).

For $a_s \gg a_s^c$, $T_c \simeq T_{\min}$ and for $a_s = a_s^c$, $T_c = T_2$. From a physical point of view, those results are clear because large positive values of a_s correspond to the depressing of the magnetization in the interface region. If the high-temperature layers are thick $[D_2/\xi_2(0) \gg 1]$, the magnetization appears in the system at $T_c \simeq T_2$. If $a_s < a_s^c$, the

If $a_s < a_s^c$, the magnetization appears on the interface already at $T_c > T_2$. In this temperature region both $a_1(T)$ and $a_2(T)$ are positive, and the solution of Eq. (3.1b) can be obtained immediately from Eq. (3.2a) by replacing therein cos by cosh

$$M_{\lambda_0}(x) = \begin{cases} \cosh\left[\frac{D_2}{2\xi_2}\right]\frac{\cosh(x/\xi_1)}{\cosh(D_1/2\xi_1)} & \text{for } |x| \leq \frac{D_1}{2} \ , \\ \cosh\left[\frac{x-D/2}{\xi_2}\right] & \text{for } \left|x-\frac{D}{2}\right| < \frac{D_2}{2} \ . \end{cases} \quad (3.4a)$$

The transition temperature is now defined by the implicit equation

$$\frac{c_1}{\xi_1(T_c)}\tanh\left[\frac{D_1}{2\xi_1(T_c)}\right] = \frac{-c_2}{\xi_2(T_2)}\tanh\left[\frac{D_2}{2\xi_2(T_c)}\right] - a_s \ . \quad (3.4b)$$

If $a_s/a_s^c \gg 1$, then taking into account that $D_2/\xi_\alpha(T_c) \gg 1$ this equation can be solved approximately and the expression for transition temperature has the form

$$T_c \simeq T_2 + \frac{a_s^2}{[(a_1'c_1)^{1/2}+(a_2'c_2)^{1/2}]^2} \ . \quad (3.4c)$$

We will not discuss this case and in the following we will put $a_s = 0$ and thus $T_1 < T_c < T_2$.

We emphasize the wide applicability of Eqs. (3.2)–(3.4), which apply as well to ferroelectrics. In Fig. 3 we show T_c as a function of $D_1/\xi_1(0)$ and $D_2/\xi_2(0)$ for GL parameters $T_1 = 16.5$ K, $T_2 = 69.15$ K, $a_1' = 110/T_1$, $a_2' = 614/T_2$, $c_1 = 178(\text{Å}^2)$, $c_2 = 515(\text{Å}^2)$, $b_1 = 5.4 \times 10^{-5}(G^{-2})$, $b_2 = 12.4 \times 10^{-5}(G^{-2})$, representing approximately bulk EuS and EuO.[20]

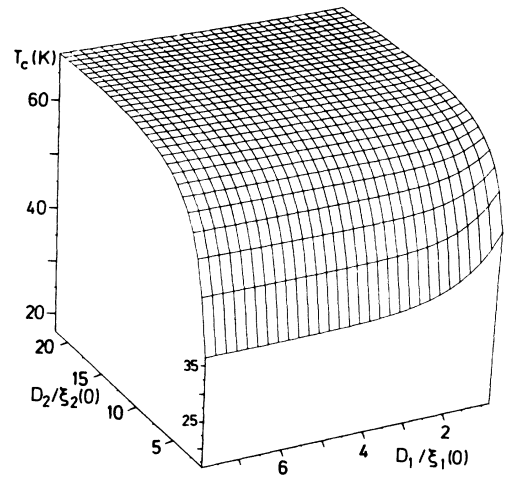

FIG. 3. Transition temperature vs thickness of the layers for material parameters of EuS/EuO with transition temperatures $T_1 = 16.5$ K, $T_2 = 69.15$ K.

B. Magnetization profile

Having determined the transition temperature, we return to the study of the magnetization profile in our multilayer system. The general solution of Eq. (2.4), which defines the magnetization profile, can be expressed through combinations of elliptic functions. Using this general solution, we have for instance computed these profiles for different temperatures, which are shown in Fig. 4. However, in some cases the solution of Eq. (2.4) can be expressed through elementary functions, namely for (i) $T \lesssim T_c$, (ii) in the case of thick layers, i.e., $D_\alpha \gg \xi_\alpha(T)$, for $T_1 < T < T_c$ and $T < T_1$, (iii) in vicinity of the lower transition temperature $T \approx T_1$.

It is clear that $M_0(x)$ is a periodic function with period D and is symmetrical around $x = 0$ and $x = D/2$.

We consider first the case (i) namely the vicinity of the

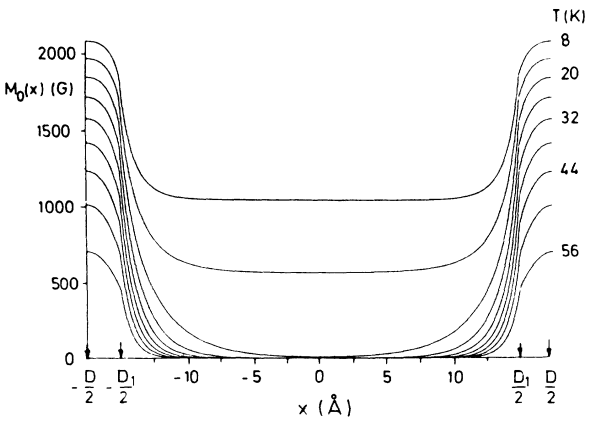

FIG. 4. Magnetization profiles of EuS/EuO layers for various temperatures and $D_1/\xi_1(0) = 19$, $D_2/\xi_2(0) = 6$.

critical point. If we expand again

$$M_0(x)=\sum_{\lambda} B_\lambda M_\lambda(x) ,$$

where the functions $M_\lambda(x)$ are defined by Eqs. (3.1a) and (3.1b), and substitute this expansion into Eq. (2.4), we obtain

$$\sum_{\lambda} \varepsilon_\lambda B_\lambda M_\lambda + b(x) \sum_{\lambda'\lambda''\lambda'''} B_{\lambda'} B_{\lambda''} B_{\lambda'''} M_{\lambda'} M_{\lambda''} M_{\lambda'''} = 0 . \tag{3.5}$$

Immediately below T_c, the condition $|B_{\lambda_0}| \gg |B_{\lambda\neq\lambda_0}|$ is fulfilled,[21] where ε_{λ_0} is the lowest (negative) eigenvalue of the operator L. Multiplying Eq. (3.5) with $M_\lambda(x)$, integrating over x, and keeping only the terms with $\lambda=\lambda'=\lambda''=\lambda'''=\lambda_0$, we get

$$B_{\lambda_0}=\left[\frac{-\varepsilon_{\lambda_0}(T)}{I_4}\right]^{1/2} , \tag{3.6a}$$

where

$$I_4=\frac{\int_{-D/2}^{D/2} M_{\lambda_0}^4(x) b(x) dx}{\int_{-D/2}^{D/2} M_{\lambda_0}^2(x) dx} . \tag{3.6b}$$

Solving Eq. (3.1b) with the boundary conditions (2.7), we obtain $M_{\lambda_0}(x)$

$$M_{\lambda_0}(x)=\begin{cases} \cos\left[\dfrac{D_2}{2\tilde{\xi}_2}\right]\dfrac{\cosh(x/\tilde{\xi}_1)}{\cosh(D_1/2\tilde{\xi}_1)} & \text{for } |x|\le\dfrac{D_1}{2} , \\ \cos\left[\dfrac{x-D/2}{\tilde{\xi}_2}\right] & \text{for } \left|x-\dfrac{D}{2}\right|<\dfrac{D_2}{2} , \end{cases} \tag{3.7}$$

where $\tilde{\xi}_\alpha=(c_\alpha/|a_\alpha-\varepsilon_{\lambda_0}(T)|)^{1/2}$. The eigenvalue $\varepsilon_{\lambda_0}(T)$ is defined by Eq. (3.2b) with the following substitutions: $\xi_\alpha\to\tilde{\xi}_\alpha$ and $a_s=0$.

If $D_1, D_2 \gg \xi_1(T)$, then from Eq. (3.2b) follows that $\varepsilon_{\lambda_0}(T)\simeq a_2'(T-T_c)$ and, hence, $B_{\lambda_0}\sim(T_c-T)^{1/2}$.

For the case (ii) the "one-mode" approximation used above is not valid anymore. However, if we consider the "thick-layer" case [$D_\alpha \gg \xi_\alpha(T)$], an elementary approximate solution can be found: In this case, for $T_1<T<T_c$ the magnetization profile $M_0(x)$ can be approximated as

$$M_0(x)\simeq\Theta\left[\frac{D_1}{2}-x\right]M_1(x)+\Theta\left[\frac{D_2}{2}-\left|x-\frac{D}{2}\right|\right]M_2(x) \tag{3.8a}$$

for $-D_1/2\le x\le -D_1/2+D$, where

$$M_1(x)=\sqrt{2}M_{1b}\left[\frac{1}{\sinh\left[\dfrac{D_1/2+x}{\xi_1}+\varphi_1\right]}+\frac{1}{\sinh\left[\dfrac{D_1/2-x}{\xi_1}+\varphi_1\right]}\right] , \tag{3.8b}$$

$$M_2(x)=M_{2b}\left[\tanh\left[\frac{x-\dfrac{D_1}{2}}{\sqrt{2}\xi_2}+\varphi_2\right]+\tanh\left[\frac{D_2+\dfrac{D_1}{2}-x}{\sqrt{2}\xi_2}+\varphi_2\right]-1\right] . \tag{3.8c}$$

Here $M_{ab}=(|a_\alpha|/b_\alpha)^{1/2}$ denotes the bulk magnetization in material α.

It is easy to check that this solution satisfies Eq. (2.4) with the maximal error of the order $\exp(-D_2/\sqrt{2}\xi_2)$, for $|x-D/2|<D_2/2$, and of the order $\exp(-3D_1/2\xi_1)$, for $|x|<D_1/2$. In order to find the integration constants φ_α, one uses the boundary conditions (2.7). This gives implicit equations for φ_α:

$$\sqrt{2}M_{1b}\left[\frac{1}{\sinh\varphi_1}+\frac{1}{\sinh\left[\dfrac{D_1}{\xi_1}+\varphi_1\right]}\right]=M_{2b}\left[\tanh\varphi_2+\tanh\left[\frac{D_2}{\sqrt{2}\varphi_2}+\varphi_2\right]-1\right] , \tag{3.9a}$$

$$\frac{2M_{2b}c_1}{\xi_1}\left[\frac{\cosh\varphi_1}{\sinh^2\varphi_1}-\frac{\cosh\left[\dfrac{D_1}{\xi_1}+\varphi_1\right]}{\sinh^2\left[\dfrac{D_1}{\xi_1}+\varphi_1\right]}\right]=\frac{M_{2b}c_2}{\xi_2}\left[\frac{1}{\cosh^2\varphi_2}-\frac{1}{\cosh^2\left[\dfrac{D_2}{\sqrt{2}\xi_2}+\varphi_2\right]}\right] . \tag{3.9b}$$

Assuming that the GL coefficients for both materials are of the same order of magnitude we readily see from (3.9) that $\varphi_\alpha \sim 0(1)$.

For $T < T_1$, the magnetization $M_0(x)$ still has the form (3.8a), but with $M_1(x)$ modified

$$M_1(x) = M_{1b}\left[\coth\left[\frac{\frac{D_1}{2}+x}{\sqrt{2}\xi_1}+\tilde{\varphi}_1\right] + \coth\left[\frac{\frac{D_1}{2}-x}{\sqrt{2}\xi_1}+\tilde{\varphi}_1\right]-1\right] . \tag{3.10}$$

The value of the constant $\tilde{\varphi}_1$ can be found again from the boundary conditions.

(iii) In the immediate vicinity of T_1 the coherence length $\xi_1(T)$ diverges and layer 1 cannot be considered to be "thick." In this temperature region $M_1(x)$ has the form

$$M_1(x) = \tilde{M}_0 nc\left[\left[\frac{b_1}{c_1}\right]^{1/2}\tilde{M}_0 x, \frac{1}{\sqrt{2}}\right] , \tag{3.11a}$$

where $nc(x,k)$ is Jacobian elliptic function.[22] The integration constant $\tilde{M}_0$ is defined again by the boundary condition. Using the realistic condition $D_1 \gg \xi_2(T_1)$, we can show that

$$\tilde{M}_0 \simeq \frac{2K\left[\frac{1}{\sqrt{2}}\right]}{D_1}\left[\frac{c_1}{b_1}\right]^{1/2} , \tag{3.11b}$$

where $K(1/\sqrt{2}) \simeq 1.854$ and is the complete elliptic integral of the first kind.[22]

It is worth noting that expressions (3.8) and (3.10) give an exponential decay of the magnetization in layer 1 near to the interface, while the expressions (3.11) predict a $1/x$ behavior.

We have also compared the exact solutions, represented in Fig. 4 with the approximate solutions, as given by expressions (3.8)–(3.11). The latter reproduce very well the magnetization profiles in the corresponding temperature regions. The magnetization profiles could be probed by neutron scattering and by local experiments.

C. Total magnetization

Now we turn to the total (average) magnetization

$$\bar{M}(T) = \int_0^D dx\, M_0(x)/D . \tag{3.12a}$$

This is shown in Fig. 5 for various values of D_2 and fixed total lattice constant D. Of course, layers with $D_\alpha \approx \xi_\alpha(0)$ are hardly realizable for magnets and bring us to the border of validity of our theory. However, this limit is of interest, because if the layers of material 2 are thin, there is a characteristic global temperature variation of the order parameter, which is more pronounced the farther they are apart. This can be understood from the fact that just below T_c, predominately, these layers are ordered.

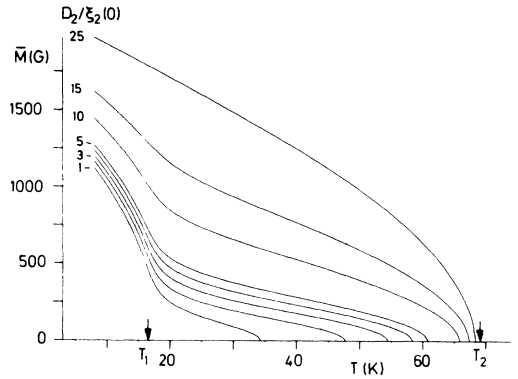

FIG. 5. Average magnetization M vs temperature for $D/\xi_2(0) = 30$ and $D_2/\xi_2(0)$ as indicated on the graph.

In the analytic presentation of the order parameter we limit ourselves to two significant temperatures. (i) Just below T_c we find, integrating the expressions (3.7), that

$$\bar{M}(T) = A(T_c - T)^{1/2} . \tag{3.12b}$$

For "thick" layers ($D_1, D_2 \gg \xi_1$)

$$A = \frac{4}{\pi\sqrt{3}}\left[\frac{a_2'}{b_2}\right]^{1/2}\frac{D_2}{D} . \tag{3.13a}$$

For "thin" layers of material 2 ($D_2 \ll \xi_1, \xi_2$ and $D_1 \gg \xi_1$), the amplitude is

$$A = 2^{3/2}\left[\frac{a_1'}{b_1}\right]^{1/2}\frac{\xi_1}{D} . \tag{3.13b}$$

The result (3.13a) is physically clear: While in the vicinity of T_c predominately the layers having the higher transition temperature are ordered, the magnetization in these layers is inhomogeneous and decreases near the interfaces. As a result, the total magnetization is reduced in comparison with its bulk value. For "thin" layers the amplitude A is very small, since the magnetization comes from regions of order ξ_1 around these layers. Clearly the power law (3.12b) is replaced by nonclassical critical behavior close to the transition.

The second characteristic quantity is the average magnetization at T_1. Using expressions (3.8a) and (3.11), after some algebra, we get

$$\bar{M}(T_1) = M_{2b}\frac{D_2}{D}\left[1+\sqrt{2}\frac{\xi_2}{D_2}\left[\frac{c_1 b_2}{c_2 b_1}\right]^{1/2}\ln\left[\frac{b_1 c_2 (D_1/\xi_2)^2}{2b_2 c_1 K^2\left[\frac{1}{\sqrt{2}}\right]\left[1+\left[\frac{c_1 b_1}{c_2 b_2}\right]^{1/2}\right]}\right]\right] . \tag{3.14}$$

The first term in (3.14) accounts for an almost homogeneously magnetized high-temperature layer, while the logarithmic term results from the $1/x$ penetration of the magnetization into the layers of material 1.

In this section we have considered mostly "thick" layers. Another interesting case is the situation of "ultrathin" layers, which is realized when the thickness of the high-temperature layer is of the order of its coherence length. In this case, one can use the so-called "δ-model" studied previously in the context of structural phase transitions.[17,19] We refer the reader to Appendix B, where the statics and dynamics of this model are considered.

IV. DYNAMICS

A. General equations of motion

In this section we consider the spin dynamics in ferromagnetic multilayer structures. Our treatment will be based on the generalized stochastic Bloch equation[14]

$$\partial_t \mathbf{M}(\mathbf{x},t)=\gamma \mathbf{M}\times\mathbf{H}_{\text{eff}}-\partial_i[\Gamma(\mathbf{x})\partial_i \mathbf{H}_{\text{eff}}] + \frac{1}{\tau(x)}\mathbf{H}_{\text{eff}}+\boldsymbol{\xi}(\mathbf{x},t)\ , \tag{4.1a}$$

with partial temporal and spatial derivatives ∂_t and ∂_x. The effective field $\mathbf{H}_{\text{eff}}=-\delta F/\delta \mathbf{M}$, where $F[\mathbf{M}]$ is the free-energy functional defined in Sec. II, and γ is the gyromagnetic ratio. The second and the third term on the right-hand side of Eq. (4.1a) are generalized diffusion and relaxation terms with space-dependent coefficients $\Gamma(\mathbf{x})$ and $\tau(\mathbf{x})$. The random force $\boldsymbol{\xi}(\mathbf{x},t)$ represents all other degrees of freedom and its fluctuations are related to the damping term in standard fashion[14]

$$\langle \xi_i(\mathbf{x},t)\xi_j(\mathbf{x}',t')\rangle = 2k_B T\delta(t-t')\cdot\left[\frac{1}{\tau(\mathbf{x})}-\nabla_{x'}\Gamma(\mathbf{x}')\nabla_{x'}\right] \times\delta(\mathbf{x}-\mathbf{x}')\delta_{ij}\ . \tag{4.1b}$$

In this paper we consider only the spin wave spectrum in the ordered low-temperature phase, $T\ll T_1$, and therefore in this section we neglect the damping and stochastic terms in Eq. (4.1a). In Sec. V, where we consider the inelastic neutron scattering, these terms will be taken into account. Equation (4.1a) together with Maxwell's equations for the demagnetization field $\mathbf{H}^m$

$$\begin{aligned}&\text{rot}\mathbf{H}^m=0\ ,\\ &\text{div}(\mathbf{H}^m+4\pi\mathbf{M})=0\ ,\end{aligned} \tag{4.2}$$

determine the spin dynamics in our system.

To analyze the harmonic motion transverse to the order parameter $\mathbf{M}_0(x)$, we linearize Eqs. (4.1) and (4.2) with respect to $\delta\mathbf{M}(\mathbf{x},t)=\mathbf{M}(x,t)-\mathbf{M}_0(\mathbf{x},t)$. Taking into account that $\mathbf{M}_0(\mathbf{x})$ points in the z direction and the static demagnetization field is zero, and denoting the demagnetization field produced by the spin wave as $\delta\mathbf{H}^m(\mathbf{x},t)$, we find for $\delta\mathbf{M}$ and $\delta\mathbf{H}^m$ the equations of motion

$$\partial_t\begin{bmatrix}\delta M_x(\mathbf{x},t)\\ \delta M_y(\mathbf{x},t)\end{bmatrix}=\gamma\begin{bmatrix}-M_0\nabla(c(x)\nabla\delta M_y)+\delta M_y\partial_x(c(x)\partial_x M_0)-M_0\delta H_y^m\\ M_0\nabla(c(x)\nabla\delta M_x)-\delta M_x\partial_x(c(x)\partial_x M_0)+M_0\delta H_x^m\end{bmatrix}, \tag{4.3a, 4.3b}$$

$$\text{rot}\delta\mathbf{H}^m=0\ , \tag{4.3c}$$

$$\text{div}(\delta\mathbf{H}^m+4\pi\delta\mathbf{M})=0\ . \tag{4.3d}$$

Because of Maxwell's equation (4.3c) one can introduce the magnetic scalar potential $\varphi^m(\mathbf{x},t)$ defined by $\delta\mathbf{H}^m(\mathbf{x},t)=-\nabla\varphi^m(\mathbf{x},t)$. Substitution of the relations $\delta\mathbf{M}(\mathbf{x},t)=\mathbf{m}(x)\exp i(\mathbf{k}_\parallel\mathbf{x}-\omega t)$ and $\varphi^m(\mathbf{x},t)=\varphi(x)\exp i(\mathbf{k}_\parallel\mathbf{x}-\omega t)$, with $\mathbf{k}_\parallel=(0,k_y,k_z)$, into Eqs. (4.3) leads to the following system of equations for $\mathbf{m}(x,t)$ and $\varphi(x)$:

$$-\frac{i\omega}{\gamma}\begin{bmatrix}m_x\\ m_y\end{bmatrix}=\begin{bmatrix}\hat{g}m_y-M_0h_y\\ -\hat{g}m_x+M_0h_x\end{bmatrix}, \tag{4.4a, 4.4b}$$

$$(\partial_x^2-k_\parallel^2)\varphi(x)=4\pi(ik_y m_y+\partial_x m_x)\ . \tag{4.4c}$$

Here the operator $\hat{g}$ is defined by

$$\hat{g}f(x)=M_0(x)[c(x)k_\parallel^2 f-\partial_x(c(x)\partial_x f)] + f\partial_x(c(x)\partial_x M_0)\ , \tag{4.5}$$

and $\mathbf{h}(x)=-(\partial_x\varphi, ik_y\varphi, ik_z\varphi)$.

If $c(x)$ as well as $M_0(x)$ are continuous functions, $\mathbf{m}(x)$, $\mathbf{h}(x)$, and their derivations are also continuous throughout the sample. We will use, however, the discontinuous approximation for $c(x)$, as it has been discussed in Sec. II. Hence, one has to consider the boundary conditions which should be imposed on $\mathbf{m}$ and $\mathbf{h}$ on the interfaces. These conditions we will derive later.

Equations (4.4) cannot be solved analytically and it is expedient to consider first some limiting cases, which admit analytical solutions.

B. Pure dipolar case

First we neglect all exchange interactions and hence we put $c(x)=0$ in (4.4). Then Eqs. (4.4a) and (4.4b) reduce to

$$-i\omega\begin{bmatrix}m_x\\ m_y\end{bmatrix}=\gamma M_0(x)\begin{bmatrix}-h_y\\ h_x\end{bmatrix}. \tag{4.6a, 4.6b}$$

Substituting **m** from Eqs. (4.6) into Eq. (4.4c), one gets the equation for the potential $\varphi(x)$

$$\left[-\partial_x^2+k_\parallel^2-\frac{4\pi\gamma}{\omega}k_y(\partial_x M_0)\right]\varphi(x)=0\ . \tag{4.7}$$

The magnetization profile $M_0(x)$ in the low-temperature region, $T\ll T_1$, is defined by expressions (3.8) and (3.10) and is shown in Fig. 4. The magnetization $M_0(x)$ assumes its bulk values M_1 and M_2 inside the layers and changes only in a narrow transition region (of the order ξ_α) near the interfaces. Integrating Eq. (4.7) from $D_1/2-\Delta/2$ to $D_1/2+\Delta/2$, with $\Delta\gg\xi_\alpha$, we get

$$\partial_x\varphi\left[\frac{D_1}{2}-\frac{\Delta}{2}\right]-\partial_x\varphi\left[\frac{D_1}{2}+\frac{\Delta}{2}\right]\simeq\frac{-4\pi\gamma}{\omega}k_y\varphi\left[\frac{D_1}{2}\right]\left[M_0\left[\frac{D_1}{2}-\frac{\Delta}{2}\right]-M_0\left[\frac{D_1}{2}+\frac{\Delta}{2}\right]\right]-k_\parallel^2\Delta\varphi\left[\frac{D_1}{2}\right], \tag{4.8}$$

where we assumed that $\varphi(x)$ is almost constant in the Δ interval. For long wave modes ($\Delta k_\parallel\ll 1$), the last term in (4.8) can be neglected. Because $M_0(D_1/2+\Delta/2)\simeq M_2$ and $M_0(D_1/2-\Delta/2)\simeq M_1$, the same boundary condition arises if one uses the approximated form for $M_0(x)$

$$M_0(x)=\sum_\alpha\sum_n M_\alpha\Theta\left[\tfrac{1}{2}D_\alpha-\left|x-\left[n+\frac{\alpha-1}{2}\right]D\right|\right], \tag{4.9}$$

and the usual electromagnetic boundary condition, namely the continuity of the normal component of $\mathbf{b}=\mathbf{h}+4\pi\mathbf{m}$ on the interfaces. The continuity of φ follows from the continuity of the tangential component of **h**.

Now we turn out attention to the solution of Eq. (4.7), which has the Bloch form, namely

$$\varphi(x+D)=e^{ik_\perp D}\varphi(x)\ , \tag{4.10}$$

with the Bloch vector $k_\perp$. For $|x|<D/2$ it is given by

$$\varphi(x)=\begin{cases}A\cosh(k_\parallel x)+B\sinh(k_\parallel x) & \text{for } |x|\le D_1/2\ ,\\ A_+\cosh[k_\parallel(x-D_1/2)]+B_+\sinh[k_\parallel(x-D_1/2)] & \text{for } D_1/2\le x\le D/2\ ,\\ A_-\cosh[k_\parallel(x+D_1/2)]+B_-\sinh[k_\parallel(x+D_1/2)] & \text{for } -D/2\le x\le -D_1/2\ .\end{cases} \tag{4.11}$$

Applying the Bloch condition (4.10) and the boundary condition (4.8) at the interfaces located at $x=\pm D_1/2$, we obtain a system of algebraic equations for the unknown coefficients A, B, $A_\pm$, and $B_\pm$. A nonzero solution of this system exists only if the determinant vanishes. This defines the dispersion relation

$$\omega^2=\frac{\gamma^2}{2}\left[\frac{4\pi k_y(M_2-M_1)}{k_\parallel}\right]^2\frac{\sinh(k_\parallel D_1)\sinh(k_\parallel D_2)}{\cosh(k_\parallel D)-\cos(k_\perp D)}\ , \tag{4.12}$$

which is shown in Fig. 6.

The coefficients A, B, $A_\pm$, and $B_\pm$ then read

$$\begin{aligned}A&=-\sinh\frac{k_\parallel D}{2}\cos\frac{k_\perp D}{2}+2i\beta\sinh\frac{k_\parallel D_2}{2}\sinh\frac{k_\parallel D_1}{2}\sin\frac{k_\perp D}{2}\ ,\\ B&=-i\cosh\frac{k_\parallel D}{2}\sin\frac{k_\perp D}{2}+2\beta\sinh\frac{k_\parallel D_2}{2}\cosh\frac{k_\parallel D_1}{2}\cos\frac{k_\perp D}{2}\ ,\end{aligned} \tag{4.13}$$

$$\begin{bmatrix}A_\pm\\ B_\pm\end{bmatrix}=\begin{bmatrix}\cosh\dfrac{k_\parallel D_1}{2} & \pm\sinh\dfrac{k_\parallel D_1}{2}\\ 2\beta\cosh\dfrac{k_\parallel D_1}{2}\pm\sinh\dfrac{k_\parallel D_1}{2} & \pm 2\beta\sinh\dfrac{k_\parallel D_1}{2}+\cosh\dfrac{k_\parallel D_1}{2}\end{bmatrix}\begin{bmatrix}A\\ B\end{bmatrix}, \tag{4.14}$$

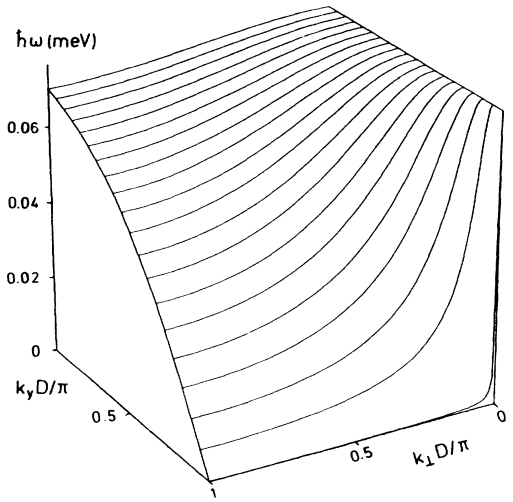

FIG. 6. Magnon dispersion relation in the pure dipolar limit, Eq. (4.12). Parameters given in the text, with $T=10$ K, $D_1=D_2=20$ Å, and $k_z=0$.

where

$$\beta=\mathrm{sgn}[k_y(M_2-M_1)]\left[\frac{\cosh(k_\parallel D)-\cos(k_\perp D)}{2\sinh(k_\parallel D_1)\sinh(k_\parallel D_2)}\right]^{1/2}. \tag{4.15}$$

In the case of "thick" layers ($k_\parallel D_\alpha \gg 1$), expressions (4.13)–(4.15) can be simplified and $\varphi(x)$ written as

$$\varphi(x)=\exp\left[-k_\parallel\left|x+\mathrm{sgn}[k_y(M_2-M_1)]\frac{D_1}{2}\right|\right] \quad \text{for } |x|\le D/2\ . \tag{4.16}$$

Because of the dependence on $\mathrm{sgn}[k_y(M_2-M_1)]$ in Eqs. (4.13)–(4.16), the form of the modes depends on the sign of k_y. This unidirectional behavior is well known and shows up in light scattering experiments.[23–25]

In Fig. 7 we show these modes for two particular directions of $\mathbf{k}$: $\mathbf{k}=(0,\pm 2\pi/D,0)$. In the long-wavelength limit ($k_\parallel D_\alpha \ll 1, k_\perp D \ll 1$) the dispersion relation (4.12)

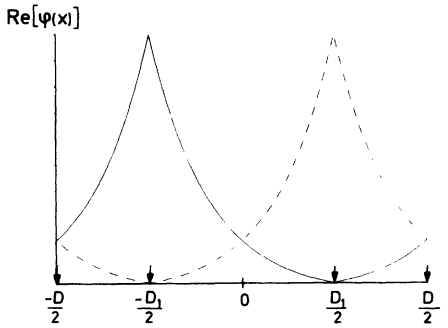

FIG. 7. Real part of the magnetic potential $\varphi(x)$. Parameters as in Fig. 6, but with $k_\perp=0$ and $|k_\parallel|=|k_y|=2\pi/D$. The solid line corresponds to $\mathrm{sgn}(k_y[M_2-M_1])>0$; the dashed line to $\mathrm{sgn}(k_y[M_2-M_1])<0$.

becomes

$$\omega^2=[4\pi(M_2-M_1)\gamma]^2\frac{D_1D_2}{D^2}\left[\frac{k_y^2}{k_\parallel^2+k_\perp^2}\right], \tag{4.17}$$

displaying the characteristic anisotropic $\mathbf{k}$ dependence for $\mathbf{k}\to 0$. The spin waves propagating in the z-x plane ($k_y^2 \ll k_\perp^2+k_z^2$) are linearly polarized along the y axis and correspond to a uniform rotation of the static magnetization in the layer plane. These are just the dipolar Goldstone modes of our multilayer system. On the other hand, the modes propagating along the y axis ($k_y^2 \gg k_\perp^2+k_z^2$) are elliptically polarized and their spectrum saturates at ω_s

$$\omega_s^2=[4\pi(M_2-M_1)\gamma]^2\frac{D_1D_2}{D}\ . \tag{4.18}$$

The modes considered here are Damon-Eshbach (DE) modes,[15] which have been studied previously in other physical systems, e.g., semi-infinite and one-layer ferromagnets[15] and multilayers consisting of alternating ferromagnetic and paramagnetic layers.[5]

C. Pure exchange case

In the pure exchange case we neglect the dipolar interaction. Then the equations of motion are given by Eqs. (4.4a) and (4.4b) with $\mathbf{h}=0$. It is convenient to introduce $m_+(x)=m_x+im_y$, which obeys

$$-M_0(x)\partial_x(c(x)\partial_x m_+)+m_+\partial_x(c(x)\partial_x M_0)+k_\parallel^2 c(x)M_0(x)m_+=\frac{\omega}{\gamma}m_+\ . \tag{4.19}$$

This equation is similar to—but not identical with—a Schrödinger equation for a particle with position-dependent effective mass in a periodic potential.

The boundary conditions for m_+ and its derivative on the interfaces can be derived from the structure of Eq. (4.19). It is easy to see that for $\omega=k_\parallel^2=0$ the solution of Eq. (4.19) is $m_+(x)=M_0(x)$. Hence $m/M_0(x)$ is a continuous function across the interfaces, even if one uses the discontinuous form (4.9) for $M_0(x)$. This condition holds also for the low-lying modes with wave lengths larger than ξ_0. This can be proved by integrating Eq. (4.19) twice around the interfaces, similarly as in the derivation of condition (4.8). Integrating Eq. (4.19) around the interface once, we obtain the boundary condition on the derivatives,

$$M_0(x)c(x)\partial_x m_+\Big|_{x=\frac{D_1^+}{2}}=M_0(x)c(x)\partial_x m_+\Big|_{x=\frac{D_1^-}{2}},$$

expressing the continuity of $M_0(x)c(x)\partial_x m_+$. This condition implies the conservation of the spin current across the boundary.

Having exposed the boundary conditions, we turn our attention to the magnon spectrum. The solutions of Eq. (4.19) have the usual Bloch form

$$m_+(x)=e^{ik_\perp x}p(x)\ ,$$

where $k_\perp$ is the Bloch wave number and $p(x+D)=p(x)$. This spectrum is shown in Fig. 8 and, as expected, has gaps at wave numbers $k_\perp$ which are multiples of π/D. A closer look at Fig. 8 reveals additional peculiarities of this spectrum, namely (i) the gaps vanish at certain points, (ii) for $k_\parallel \neq 0$ the bands are narrow in the low-energy region and wide in the high-energy one. The discussion below is organized as follows. First, we explain the vanishing of gaps and show that this is a generic property of the magnon spectrum in the pure exchange limit. Second, we indicate how the dispersion relation is computed and present some simple physical arguments explaining how the bandwidths can be understood solely from the dispersion relations of the bulk constituents. Third, using the analytical form of the dispersion relation we identify the points in $(\mathbf{k},\omega)$ space where the gaps vanish and for $k_\parallel=0$ discuss the $k_\perp$ dependence of the gaps.

The vanishing of gaps can be understood in the following way. Because Eq. (4.19) is similar to a Schrödinger equation, the last term on the left-hand side can be considered as a "potential energy" which depends on the parameter $k_\parallel^2$. On the other hand, because $k_\parallel$ appears in Eq. (4.19) only in quadratic form, this equation is invariant with respect to a C_2 symmetry operation around the z axis. From this symmetry it follows that at the band edges the solutions have definite parity. One can also show that for adjacent band edges these parities are different.[26,27] It is worth noting at this point, that in the pure dipolar case the spin dynamics equation (4.4c) is not invariant with respect to the symmetry operation discussed above and the solutions do not have definite parity.

It is well known that in diatomic molecules terms, the wave functions of which have different parity,[28] can cross. Because Eq. (4.19) is not identical with the usual Schrödinger equation, it is necessary to show how the arguments leading to the term crossing in diatomic molecules can be applied in the present situation. Equation (4.19) can be written in the form

$$\hat{g}(k_\parallel^2)m_+ = \frac{\omega}{\gamma} m_+ \ , \tag{4.19a}$$

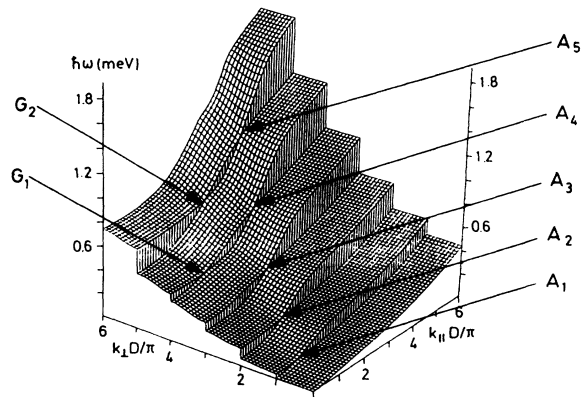

FIG. 8. Magnon dispersion relation in the pure exchange limit. Parameters given in Fig. 6. The points A_i, G_i are defined in the text.

where the operator $\hat{g}$ contains the parameter $k_\parallel^2$. If one defines the scalar product of two functions $m_{+1}(x)$ and $m_{+2}(x)$ by

$$\langle m_{+i}|m_{+j}\rangle = \lim_{L\to\infty}\frac{1}{L}\int_{-L/2}^{L/2}\frac{dx}{M_0(x)} m^*_{+i}(x)m_{+j}(x), \tag{4.19b}$$

the operator $\hat{g}$ is Hermitian and its matrix elements have the form

$$\langle m_{+i}|\hat{g}m_{+j}\rangle = \lim_{L\to\infty}\frac{1}{L}\int_{-L/2}^{L/2}\frac{dx}{M_0(x)} m^*_{+i}(x)\hat{g}m_{+j}(x) \ . \tag{4.19c}$$

Suppose we solved Eq. (4.19a) for some value $k_{\parallel 0}^2$ and obtained a gap $\delta\omega=\omega_1-\omega_2$ between the upper and lower frequencies ω_1 and ω_2. The eigensolutions corresponding to these frequencies are $m_{+1}(x)$ and $m_{+2}(x)$. For a slight change of the parameter $k_\parallel^2$ to the new value $k_\parallel^2=k_{\parallel 0}^2+\delta k_\parallel^2$, the operator $\hat{g}(k_\parallel^2)$ reads up to the first order in $\delta k_\parallel^2$

$$\hat{g}(k_\parallel^2)=\hat{g}(k_{\parallel 0}^2)+\delta\hat{g} \ . \tag{4.19d}$$

The solution of Eq. (4.19a) is represented in the form $m_+(x)=c_1 m_{+1}(x)+c_2 m_{+2}(x)$, which after substitution into Eq. (4.19a) and projection onto m_{+1} and m_{+2} leads to the usual secular equation. From this we obtain the new band edges

$$\frac{\omega_{1,2}^n}{\gamma} = \tfrac{1}{2}(\omega_1+\omega_2+\delta G_{11}+\delta G_{22}) \pm [\tfrac{1}{4}(\omega_1-\omega_2+\delta G_{11}-\delta G_{22})^2+|\delta G_{12}|^2]^{1/2} \ , \tag{4.19e}$$

where

$$\delta G_{ij}=\frac{\langle m_{+i}|\delta\hat{g}|m_{+j}\rangle}{(\langle m_{+i}|m_{+i}\rangle\langle m_{+j}|m_{+j}\rangle)^{1/2}} \quad \text{with } i,j=1,2 \ . \tag{4.19f}$$

Hence, a gap vanishes if both

$$\omega_1-\omega_2+\delta G_{11}-\delta G_{22}=0 \tag{4.19g}$$

and

$$\delta G_{12}=0 \ . \tag{4.19h}$$

As mentioned before, the eigensolutions for adjacent band edges have opposite parity and therefore the matrix element δG_{12} vanishes and the condition (4.19h) is always satisfied. Condition (4.19g) can be satisfied for special values of $k_\parallel^2$ and hence gaps can vanish.

Now we indicate how the dispersion relation and its gaps are computed. Generalizing the usual treatment[27] to x-dependent stiffness $c(x)$, we determine even and odd one cell solutions $g(\omega,x)$ and $u(\omega,x)$ of Eq. (4.19). In terms of these the dispersion relation follows from

$$\cos k_\perp D = 1+2u(\omega,D/2)\partial_x g(\omega,D/2)c_2/W \ , \tag{4.20a}$$

with the Wronskian $W=c_1 g(\omega,0)\partial_x u(\omega,0)$. Equation (4.20a) can be written also in the form

$$\cos k_\perp D = -1+2g(\omega,D/2)\partial_x u(\omega,D/2)c_2/W \ . \quad (4.20b)$$

One sees from Eqs. (4.20) that the zeros of $u(\omega,D/2)$, $\partial_x g(\omega,D/2)$, $g(\omega,D/2)$, and $\partial_x u(\omega,D/2)$, viewed as functions of ω, define the band edges. The adjacent band edges correspond to the zeros of $u(\omega,D/2)$ and $\partial_x g(\omega,D/2)$ or $g(\omega,D/2)$ and $\partial_x u(\omega,D/2)$. Thus gaps disappear if $u(\omega,D/2)$ and $\partial_x g(\omega,D/2)$ or $g(\omega,D/2)$ and $\partial_x u(\omega,D/2)$ vanish simultaneously for the same value of ω. To elucidate this phenomenon we consider again "thick" layers and use the discontinuous form for $M_0(x)$ (4.9). Now the solution of Eq. (4.19) is elementary. Using the boundary conditions discussed above, one finds

$$g(\omega,x)=\begin{cases}\cos(p_1 x) & \text{for } 0\le x\le D_1/2,\\ \dfrac{M_2}{M_1}\left\{\cos\dfrac{p_1 D_1}{2}\cos\left[p_2\left[x-\dfrac{D_1}{2}\right]\right]-\dfrac{M_1^2 c_1 p_1}{M_2^2 c_2 p_2}\sin\dfrac{p_1 D_1}{2}\sin\left[p_2\left[x-\dfrac{D_1}{2}\right]\right]\right\} & \text{for } D_1/2\le x\le D/2\ ,\end{cases} \quad (4.12a)$$

and

$$u(\omega,x)=\begin{cases}\sin(p_1 x) & \text{for } 0\le x\le D_1/2\\ \dfrac{M_2}{M_1}\left\{\sin\dfrac{p_1 D_1}{2}\cos\left[p_2\left[x-\dfrac{D_1}{2}\right]\right]+\dfrac{M_1^2 c_1 p_1}{M_2^2 c_2 p_2}\cos\dfrac{p_1 D_1}{2}\sin\left[p_2\left[x-\dfrac{D_1}{2}\right]\right]\right\} & \text{for } D_1/2\le x\le D/2\ ,\end{cases} \quad (4.21b)$$

where $p_\alpha=[(\omega/c_\alpha M_\alpha\gamma)-k_\parallel^2]^{1/2}$. These expressions are valid also for purely imaginary p_α with corresponding change of $\cos(p_\alpha x)$ into $\cosh(|p_\alpha|x)$, etc.

In order to understand the bandwidths let us first consider the dispersion relations in the homogeneous materials 1 and 2, namely $\omega_\alpha=\gamma c_\alpha M_\alpha(k_\perp^2+k_\parallel^2)$. These are shown in Fig. 9 for a fixed value $k_\parallel$ under the assumption $c_2M_2>c_1M_1$. In the frequency region $\gamma c_1 M_1 k_\parallel^2<\omega<\gamma c_2 M_2 k_\parallel^2$ the spin waves propagate freely in layer 1, but penetrate only exponentially into layer 2. This situation is similar to the tight-binding model of electron theory. The spin waves in layers 1 with exponentially decaying tail into layers 2 play the role of the atomic wave functions. The bandwidth depends on the overlap of these "atomic" functions and goes as $\exp(-|p_2|D_2)$ in this frequency region. For "wide" layers 2, the bands are narrow and the gaps are wide and do not vanish. It is worth mentioning that these "tight-binding" gaps exist only for $k_\parallel\neq 0$.

In the frequency region $\omega>\gamma c_2 M_2 k_\parallel^2$ the spin waves propagate freely in both layers and, as a result, the bands are wide. In this frequency region gaps disappear at certain values of ω and $k_\parallel$, as has been discussed above.

Now we can identify the points in (k,ω) space where the gaps vanish. Using expressions (4.21a) and (4.21b) and the condition that $u(\omega,D/2)$ and $\partial_x g(\omega,D/2)$ or $g(\omega,D/2)$ and $\partial_x u(\omega,D/2)$ should vanish simultaneously, we find that the gaps vanish whenever p_1 and p_2 obey either the condition

$$p_1 D_1 = n\pi \ \text{ and } \ p_2 D_2 = m\pi\ , \quad (4.22a)$$

or

$$p_1 D_1 + p_2 D_2 = n\pi \ \text{ and } \ \omega=\gamma k_\parallel^2\frac{M_1^4 c_1^2 - M_2^4 c_2^2}{M_1^3 c_1 - M_2^3 c_2}\ , \quad (4.22b)$$

with positive integers n and m. In Fig. 8 at the points A_1 to A_5, condition (4.22b), with $n=1-5$, is satisfied, while at the points G_1 and G_2 condition (4.22a) holds, with $n=3, m=1$ and $n=4, m=1$, respectively.

Using expressions (4.21a) and (4.21b) we can also calculate the gap widths. It is easy to show that for $k_\parallel=0$ and small D_2 and $k_\perp$ the gaps are proportional to $k_\perp^2$, which is

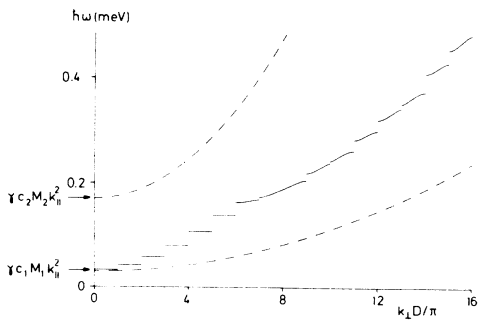

FIG. 9. Magnon dispersion relation in the exchange limit for the multilayer structure (solid) compared with the homogeneous dispersion relations (dashed). Parameters are as in Fig. 6, but with $D_1=D_2=80$ Å and $(k_\parallel D/\pi)=8$.

in accordance with the results of the hydrodynamical theory.

To conclude this section, we want to point out that the gap vanishing phenomenon is a generic property of Eq. (4.19), which is not restricted to the "step form" for $M_0(x)$. It follows solely from the structure of Eq. (4.19) and does not depend on the particular form of $M_0(x)$. In Appendix B we show that the gaps may vanish also in the "δ model," where the static magnetization $M_0(x)$ is a continuous function. We also refer the reader to Ref. 21, where the gradual change of the magnetization in the transition region between the layers is taken into account.

D. Exchange and dipolar interaction

Having considered the two limiting cases, we turn our attention now to the general case, with both exchange and dipolar interactions included. The spin wave dynamics is described by Eqs. (4.4) and the boundary conditions for $\mathbf{m}$ following therefrom require that $\mathbf{m}/M_0(x)$ and $M_0(x)c(x)\partial_x\mathbf{m}$ are continuous across the interfaces. Equation (4.4c) can be solved analtyically with the result[18,29]

$$\varphi(x)=2\pi\int_{-\infty}^{\infty}dx' e^{-k_{\parallel}|x'-x|}\times\left[\frac{ik_y}{k_{\parallel}}m_y(x')-\mathrm{sgn}(x'-x)m_x(x')\right]. \tag{4.23}$$

Substituting (4.23) into Eqs. (4.4a) and (4.4b), we obtain an integro-differential equation for $\mathbf{m}$

$$\frac{\omega}{\gamma}\mathbf{m}=\hat{H}(\mathbf{m})\equiv\begin{bmatrix}0 & i\hat{g}\\ -i(\hat{g}+4\pi M_0) & 0\end{bmatrix}\mathbf{m}+2\pi i k_{\parallel}M_0(x)\int_{-\infty}^{\infty}dx' e^{-k_{\parallel}|x'-x|}\times\begin{bmatrix}i\,\mathrm{sgn}(x-x')\sin\alpha & \sin^2\alpha\\ 1 & -i\,\mathrm{sgn}(x-x')\sin\alpha\end{bmatrix}\mathbf{m}(x'), \tag{4.24}$$

where $\sin\alpha=k_y/k_{\parallel}$ and the operator $\hat{g}$ is defined in (4.5). We will not discuss here the properties of the linear operator $\hat{H}$, but refer the reader to the standard textbooks.[30]

We solved Eq. (4.24) numerically for different directions of $\mathbf{k}_{\parallel}$ with $M_0(x)$ given by expression (4.9). In Appendix C the reader can find the details of the numerical calculations.

For $\mathbf{k}=(k_{\perp},0,k_{\parallel})$ the dispersion relation (solid lines) is shown in Fig. 10. For comparison, in the same figure we have also drawn the dispersion relation for the pure exchange case (broken lines). We see that they are qualitatively similar and in particular there are also points where the gaps vanish. This similarity is intuitively clear: For these particular wave vectors $\mathbf{k}$ the Hamiltonian is invariant with respect to the C_2 symmetry operation around the z axis as is the case in pure exchange limit. Had we picked materials with higher transition temperatures, the quantitative difference would have been even smaller. Roughly speaking, the pure exchange theory applies for wave vectors such that the spin wave energy is large compared to the demagnetization energy, i.e., $c_\alpha k^2 \gg 4\pi$.

For $\mathbf{k}=(k_{\perp},k_{\parallel},0)$ the dispersion relation is shown in Fig. 11 (solid lines). The comparison with the pure exchange case (dashed lines) shows that previously degenerate levels now split (point A). This level splitting can be understood because the C_2 symmetry is broken for $k_y\neq 0$.

Another characteristic feature of the dispersion relations are the strong peaks at $k_{\perp}=2\pi n/D$ and the singular directional dependence on $\mathbf{k}$ for $\mathbf{k}\to 0$, in contrast to the

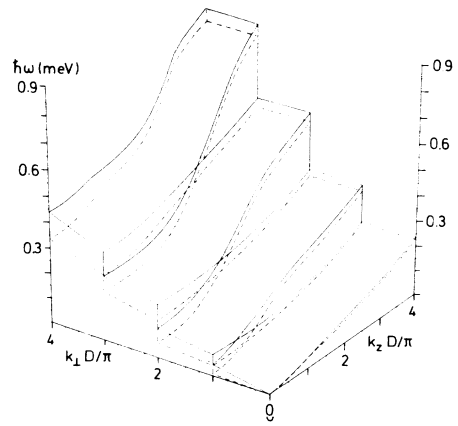

FIG. 10. Spin wave frequency at the zone boundaries including the demagnetization energy (solid) compared with the pure exchange case (dashed) for the special wave vector section $(k_{\perp},0,k_z)$. $D_1=D_2=20$ Å.

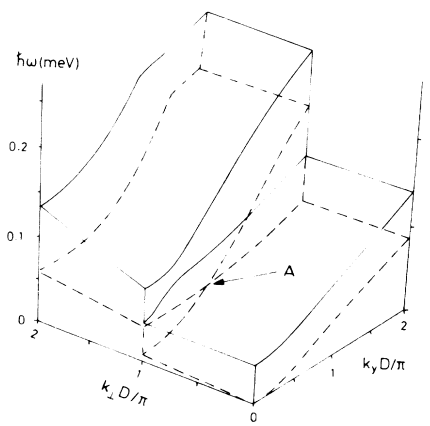

FIG. 11. Spin wave frequencies as in Fig. 10, but now for the wave vector section $(k_{\perp},k_y,0)$. Level splitting is clearly seen in point A.

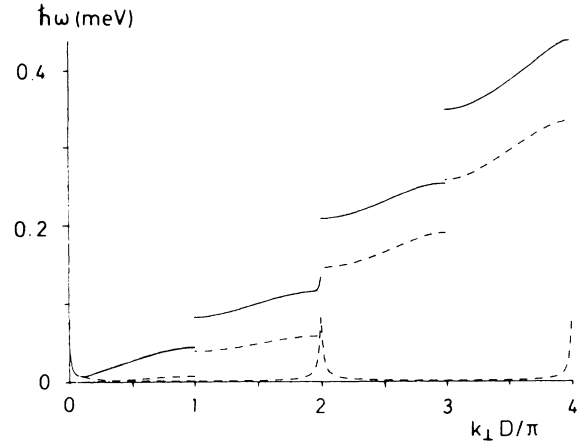

FIG. 12. Magnon dispersion vs $k_\perp D/\pi$ for $k_y D/\pi=0.01$, $k_z=0$, and $D_1=D_2=20$ Å. The pure dipolar limit is represented by the dashed, the pure exchange limit by the dash-dotted, and the general case by the solid lines.

pure exchange spectrum. In Fig. 12 we show the magnon dispersion relation in the particular direction $\mathbf{k}=(k_\perp,0.01\pi/D,0)$, (a) for pure dipolar interaction (dashed lines), (b) for pure exchange interaction (dash-dotted lines) as well as (c) the general case (solid lines). From comparison of the general case with the dipolar dispersion relation we see that the peaks can be explained as arising from the dipolar interactions.

In Appendix C the reader finds some details concerning the computation of the dispersion relation.

V. INELASTIC NEUTRON SCATTERING CROSS SECTION

The magnon dispersion relation calculated in this paper can be probed by inelastic neutron scattering experiments. Because in these experiments the "high" energy part ($\omega \gtrsim 4\pi\gamma M_0$) of this spectrum is studied, in the derivation of the cross section it is sufficient to consider the pure exchange limit only. It is well known[31] that the differential cross section for inelastic magnon scattering of nonpolarized neutrons is given by

$$\frac{d^2\sigma}{d\Omega\, dE'} = A\frac{\kappa'}{\kappa}\sum_{\alpha,\beta}(\delta_{\alpha\beta}-\hat{q}_\alpha\hat{q}_\beta) \times\int\int\langle m_\alpha(\mathbf{x},\omega)m_\beta(\mathbf{x}',-\omega)\rangle \times e^{-i\mathbf{q}(\mathbf{x}-\mathbf{x}')}d\mathbf{x}\,d\mathbf{x}' , \tag{5.1}$$

where

$$m_\alpha(\mathbf{x},\omega)=\int m_\alpha(\mathbf{x},t)e^{i\omega t}dt ,$$

A is constant, $\boldsymbol{\kappa}$ and $\boldsymbol{\kappa}'$ are the wave vectors of incident and scattered neutrons, $\mathbf{q}=\boldsymbol{\kappa}-\boldsymbol{\kappa}'$ and $\hat{q}_\alpha=q_\alpha/q$.

The energies of the incident and scattered neutrons are E and E' and $\omega=E'-E$. Because of the continuum approach used through this paper the magnetic form factor and the Debye-Waller factor do not appear in the expression (5.1). From the symmetry of our problem, it is obvious that

$$\langle m_x(\mathbf{x},\omega)m_x(\mathbf{x},-\omega)\rangle=\langle m_y(\mathbf{x},\omega)m_y(\mathbf{x}',-\omega)\rangle , \tag{5.2a}$$

$$\langle m_x(\mathbf{x},\omega)m_y(\mathbf{x}',-\omega)\rangle=-\langle m_y(\mathbf{x},\omega)m_x(\mathbf{x}',-\omega)\rangle . \tag{5.2b}$$

In linear spin wave theory, which is considered in this paper, the correlation functions $\langle m_\alpha(\mathbf{x},\omega)m_z(\mathbf{x}',-\omega)\rangle = \langle m_z(\mathbf{x},\omega)m_\alpha(\mathbf{x}',-\omega)\rangle=0$, with $\alpha=x,y,z$. Because our system is translational invariant in the plane parallel to the layers, the correlation functions can be written as

$$\langle m_\alpha(\mathbf{x},\omega)m_\beta(\mathbf{x}',-\omega)\rangle=\frac{1}{(2\pi L)^2}\int\langle m_\alpha(x,q_\parallel,\omega)m_\beta(x',-q_\parallel,-\omega)\rangle e^{i\mathbf{q}_\parallel(\mathbf{x}_\parallel-\mathbf{x}'_\parallel)}d\mathbf{q}_\parallel , \tag{5.3}$$

with $\mathbf{x}=(x,\mathbf{x}_\parallel)$ and $\mathbf{q}=(q_\perp,\mathbf{q}_\parallel)$. Substituting (5.2) and (5.3) into (5.1) we obtain

$$\frac{d^2\sigma}{d\Omega\, dE'}=A\frac{\kappa'}{\kappa}(1+\hat{q}_z^2)\int\int\langle m_x(x,q_\parallel,\omega)m_x(x',-q_\parallel,-\omega)\rangle e^{-iq_\perp(x-x')}dx\,dx' . \tag{5.4}$$

The classical fluctuation dissipation theorem[14] relates the correlation function $\langle m_\alpha(x,q_\parallel,\omega)m_\beta(x',-q_\parallel,-\omega)\rangle$ to the linear response function $G_{xx}(x,x',q_\parallel,\omega)$

$$\langle m_x(x,q_\parallel,\omega)m_x(x',-q_\parallel,-\omega)\rangle = \frac{2k_BT}{\omega}\,\mathrm{Im}G_{xx}(x,x',q_\parallel,\omega) . \tag{5.5}$$

The linear response functions $G_{\alpha\beta}(x,x',q_\parallel,\omega)$ describe the response of the magnetization $\mathbf{m}(x,q_\parallel,\omega)$ to a weak external magnetic field $\mathbf{h}(x,q_\parallel,\omega)$

$$\langle m_\alpha(x,q_\parallel,\omega)\rangle=\int G_{\alpha\beta}(x,x',q_\parallel,\omega)h_\beta(x',q_\parallel,\omega)dx' , \tag{5.6}$$

and can be calculated from the equation of motion (4.1a).

First we will neglect the diffusion term in Eq. (4.1), whose influence on the final results will be discussed later. Then is is easy to show that the response functions $G_{\alpha\beta}$ obey the following matrix equation:

$$\hat{M}_{\alpha\beta}(x)G_{\beta\nu}(x,x',q_\parallel,\omega)=\delta_{\alpha\nu}\delta(x-x'),\quad \alpha,\beta,\nu=x,y , \tag{5.7a}$$

where

$$\hat{M}_{xx}(x)=\hat{M}_{yy}(x)=\frac{-i\omega/\tau(x)}{\tau^{-2}(x)+(\gamma M_0(x))^2} + \frac{1}{M_0(x)}\hat{g}(x,q_\parallel) \tag{5.7b}$$

$$\hat{M}_{xy}(x)=-\hat{M}_{yx}(x)=\frac{-i\omega\gamma M_0(x)}{\tau^{-2}(x)+(\gamma M_0(x))^2} . \quad (5.7c)$$

The operator $\hat{g}(x,q_\parallel)$ was defined previously, Eq. (4.5). If we define

$$G_\pm(x,x',q_\parallel,\omega)=G_{xx}(x,x',q_\parallel,\omega)\pm iG_{yx}(x,x',q_\parallel,\omega) , \quad (5.8)$$

then it is easy to see from Eqs. (5.7) that $G_\pm$ obey the equations

$$\frac{1}{\gamma M_0(x)}\left[\frac{\mp\omega}{1\mp\frac{i}{\gamma\tau(x)M_0(x)}}+\gamma\hat{g}(x,q_\parallel)\right]G_\pm(x,x',q_\parallel,\omega)=\delta(x-x') . \quad (5.9)$$

Hence

$$G_-(x,x',q_\parallel,\omega)=G_+^*(x,x',q_\parallel,-\omega) , \quad (5.10)$$

and from Eqs. (5.8) and (5.10) we obtain

$$G_{xx}(x,x',q_\parallel,\omega)=\tfrac{1}{2}[G_+(x,x',q_\parallel,\omega)+G_+^*(x,x',q_\parallel,-\omega)] . \quad (5.11)$$

Let us introduce the functions $m_n(x,\mathbf{k})$ and $\tilde{m}_n(x,\mathbf{k})$ with $\mathbf{k}=(k_\perp,\mathbf{k}_\parallel)$, which obey the following eigenvalue equations:

$$\left[-\varepsilon_n(\mathbf{k})+\left[1-\frac{i}{\gamma\tau(x)M_0(x)}\right]\gamma\hat{g}(x,k_\parallel)\right]m_n(x,\mathbf{k})=0 , \quad (5.12a)$$

$$\left[-\varepsilon_n^*(\mathbf{k})+\left[1+\frac{i}{\gamma\tau(x)M_0(x)}\right]\gamma\hat{g}(x,k_\parallel)\right]\tilde{m}_n(x,\mathbf{k})=0 , \quad (5.12b)$$

and the boundary conditions

$$m_n(x+D,\mathbf{k})=e^{ik_\perp D}m_n(x,\mathbf{k}) , \quad (5.13a)$$

$$\tilde{m}_n(x+D,\mathbf{k})=e^{ik_\perp D}\tilde{m}_n(x,\mathbf{k}) . \quad (5.13b)$$

Here $k_\perp$ lies in the first Brillouin zone and $n=0,1\ldots$ numbers the energy bands.

Using these functions we can write the response function G_+ in the following form:[30]

$$G_{xx}(x,x',k_\parallel,\omega)=\lim_{L\to\infty}\frac{\gamma}{L}\times\sum_{k_\perp,n}\frac{\tilde{m}_n^*(x',\mathbf{k})m_n(x,\mathbf{k})}{[\varepsilon_n(\mathbf{k})-\omega]\langle\tilde{m}_n(\mathbf{k})|m_n(\mathbf{k})\rangle} , \quad (5.14)$$

where the scalar product is defined as

$$\langle\tilde{m}_n(\mathbf{k})|m_n(\mathbf{k})\rangle=\lim_{L\to\infty}\frac{\gamma}{L}\int_{-L/2}^{L/2}\frac{\tilde{m}_n^*(x,\mathbf{k})m_n(x,\mathbf{k})dx}{M_0\left[1-\frac{i}{\gamma\tau M_0}\right]} . \quad (5.15)$$

For every given $\tau(x)$ and $M_0(x)$ one can solve Eq. (5.12) numerically and calculate the differential cross section using Eqs. (5.4), (5.5), (5.11), and (5.14).[32]

In Fig. 13 we display the cross section as a function of ω and $q_\perp$ for fixed $q_\parallel=0$. Here $\tau(x)$ is chosen to have a "step form"

$$\tau(x)=\sum_{n=-\infty}^{\infty}\sum_{\alpha=1,2}\tau_\alpha\Theta\left[\tfrac{1}{2}D_\alpha-\left|x-\left[n+\frac{\alpha+1}{2}\right]D\right|\right] . \quad (5.16)$$

The spin-wave band structure is clearly seen in this figure. In Fig. 14 we also plot the cross section as a function of ω and $q_\parallel$ for fixed $q_\perp=2\pi/D$. We see that the cross section is enhanced at the point A_2. Comparison with Fig. 8 shows that this is one of the values of ω and $q_\parallel$ where the gap in the spin wave spectrum vanishes. Hence this is a possibility to identify by inelastic neutron scattering experiments the vanishing of gaps, predicted in our theory.

To obtain the line shape of the cross section and to understand the increase of the cross section at the points of vanishing gaps, we note first that for $\tau(x)\to\infty$ Eq. (5.12a) reduces to the spin wave equation (4.19) and hence $\tilde{m}_n^0(x,\mathbf{k})=m_n^0(x,\mathbf{k})$, with real $\varepsilon_n^0(\mathbf{k})$. For large $\tau(x)$, Eq. (5.12a) can be solved perturbatively and we obtain in first-order perturbation theory that

$$\varepsilon_n(\mathbf{k})=\varepsilon_n^0(\mathbf{k})-i\bar{\gamma}_n^R(\mathbf{k}) , \quad (5.17a)$$

where

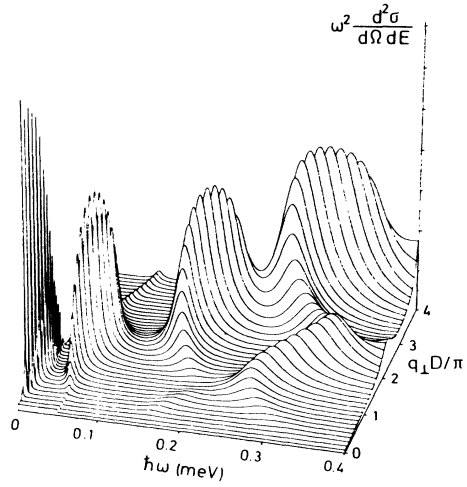

FIG. 13. Neutron scattering cross section (times the square of the energy transfer ω) in arbitrary units as a function of ω and momentum transfer $q_\perp$ along the staple axis. The relaxation times τ_α are chosen $\tau_\alpha=10/(\gamma M_\alpha)$, $\alpha=1,2$, and $\Gamma=0$.

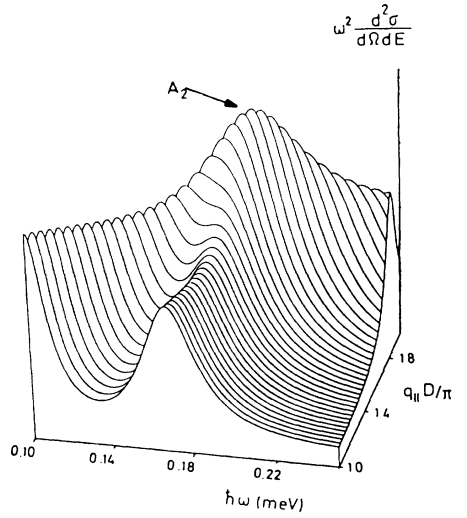

FIG. 14. Neutron scattering cross section (times the square of energy transfer ω) in arbitrary units as a function of ω and momentum transfer $q_\parallel$ within the layer planes with $q_\perp = 2\pi/D$. The gap vanishing effect is seen in point A_2 (compare with Fig. 8).

$$\bar{\gamma}_n^R(\mathbf{k}) = \varepsilon_n^0(\mathbf{k}) \frac{1}{\gamma D} \int_{-D/2}^{D/2} \frac{|m_n^0(x,\mathbf{k})|^2}{M_0^2(x)\tau(x)} dx \ . \tag{5.17b}$$

The eigenfunctions $m_n^0(x,\mathbf{k})$ are assumed to be normalized to unity according to definition (4.19b).

If we expand $m_n^0(x,\mathbf{k})$ in the form

$$m_n^0(x,\mathbf{k}) = e^{ik_\perp x} \sum_\nu p_n(\nu,\mathbf{k}) e^{i2\pi\nu x/D}, \quad \nu = 0, \pm 1, \pm 2, \ldots , \tag{5.18}$$

then, after some algebra, we obtain for frequencies ω close to $\varepsilon_n^0(\mathbf{k})$

$$\frac{d^2\sigma}{d\Omega\, dE'} = A' \frac{\kappa'}{\kappa}(1+\hat{q}_z^2) \times \sum_n \frac{|p_n(n_0,\mathbf{k})|^2 \varepsilon_n^0(\mathbf{k}) \bar{\gamma}_n^R(\mathbf{k})}{(\omega^2 - \varepsilon_n^0(\mathbf{k})^2)^2 + (2\varepsilon_n^0(\mathbf{k})\bar{\gamma}_n^R(\mathbf{k}))^2} , \tag{5.19}$$

where all constants have been subsumed in A'. Here $\mathbf{k} = (k_\perp, q_\parallel)$, $k_\perp = q_\perp \mathrm{mod}(2\pi/D)$, and $n_0 = D(q_\perp - k_\perp)/2\pi$. From the expression (5.19) it is easy to see how the vanishing of gaps influences the cross section. If we are far from the point in $(\mathbf{q},\omega)$ space, where the gap in the spin wave spectrum vanishes, then for $\bar{\gamma}_n^R \to 0$ only one term in expression (5.19) effectively contributes to the cross section. However, at the points where the gap vanishes, two terms, coming from two adjacent bands, have the same order of magnitude and both contribute to the cross section. This leads to the increase seen in Fig. 14.

At this point we want to discuss the influence of the diffusion term, which has been neglected so far. If we keep the diffusion term in the spin dynamic equation (4.1), we obtain the following equation for $m_n(x,\mathbf{k})$:

$$\left[-\varepsilon_n(\mathbf{k}) + \left[1 - \frac{i}{\gamma\tau M_0} \right] \gamma \hat{g}(x,k_\parallel) + i[\partial_x \Gamma(x)\partial_x - q_\parallel^2 \Gamma(x)] \frac{1}{M_0} \hat{g}(x,k_\parallel) \right] m_n(x,\mathbf{k}) = 0 \ . \tag{5.20}$$

The last term in this equation contributes to the imaginary part of $\varepsilon_n(\mathbf{k})$ and we get

$$\varepsilon_n(\mathbf{k}) = \varepsilon_n^0(\mathbf{k}) - i[\bar{\gamma}_n^R(\mathbf{k}) + \bar{\gamma}_n^D(\mathbf{k})] \ . \tag{5.21}$$

In the first order of perturbation theory

$$\bar{\gamma}_n^D(\mathbf{k}) = \frac{\varepsilon_n^0(\mathbf{k})}{\gamma} \frac{1}{D} \int_0^D \Gamma(x) \left[k_\parallel^2 \left| \frac{m_n^0(x,\mathbf{k})}{M_0} \right|^2 + \left| \partial_x \left[\frac{m_n^0(x,\mathbf{k})}{M_0} \right] \right|^2 \right] dx \ . \tag{5.22}$$

For $\mathbf{k} \to 0$ we know that $m_0(x,\mathbf{k}) \sim M_0(x)$ and $\varepsilon_0(\mathbf{k}) \sim k^2$. Hence we see from (5.22) that for $\mathbf{k} \to 0$ $\bar{\gamma}_0^D(k) \sim 0(k^4)$ and in this limit the result (5.19) is valid. The range of wave vectors for which k^2 or k^4 behavior can be observed, depends on the material parameters such as the diffusion constant Γ and the relaxation time τ. In the Heisenberg ferromagnets, a good example of which are EuO and EuS, the relaxation time τ is very large and hence the linewidth is proportional k^4.[20] That we keep only the relaxation term is motivated mainly by computational convenience and is sufficient to exhibit the peak structure of the neutron scattering cross section in Fig. 14.

VI. SUMMARY AND DISCUSSION

The results of the preceding sections describe the statics and dynamics in ferromagnetic superlattices. The theory is based on an inhomogeneous Ginzburg-Landau (GL) free-energy functional with position-dependent GL coefficients. The form of these coefficients models periodically alternating layers with different transition temperatures T_1 and T_2 and can incorporate different interface interactions.

The transition temperature T_c of a ferromagnetic superlattice depends on the layer thicknesses D_1 and D_2 as well as on the strength of the interface interactions. If these interactions depress the magnetization in the interface region, the transition temperature always lies below T_2. The transition temperature almost coincides with T_2 for thick high-temperature layers ($D_2/\xi_2(0) \gg 1$), but substantially deviates from it for thin layers whose thicknesses are of order of several coherence lengths [$D_2 \approx \xi_2(0)$]. On the other hand, if the interface interactions support the ferromagnetic order at higher temperatures than T_2, the phase transition in the superlattice can appear at $T_c > T_2$. The temperature shift depends on the strength of interface interactions and its experimental verification can give important information about interface properties. Because the derivation of the equation for T_c is material independent, this equation is also appl-

icable to other systems undergoing phase transitions as ferroelectrics, etc.

The magnetization profile can be found from the GL equation and is generally given by a combination of elliptic functions. In some physically relevant cases elementary analytical expressions can be obtained, namely (1) in the vicinity of the transition temperature T_c, where the magnetization profile can be found by means of "one-mode" approximation and where the mean field result for the temperature dependence of the spontaneous magnetization has been recovered; (2) the temperature region $T_1 \ll T < T_c$, where the magnetization has its bulk value deep inside of the high temperature layer, but decays exponentially near the interface, penetrating into the lower temperature one; (3) the temperature region $T \ll T_1$, where the magnetization reaches its bulk values in every layer far from the interface and changes rapidly in the transition region (of order of bulk coherence lengths) near to it; (4) the immediate vicinity of T_1, where the bulk coherence length ξ_1 diverges and the low-temperature layer is effectively "thin" ($D_1 \ll \xi_1$). In this temperature region the magnetization penetration into the low temperature layer is described by a $1/x$ law. These different magnetization profiles could be probed by means of local experiments.

The temperature dependence of the average magnetization in superlattices has a characteristic form depending on the thicknesses of layers. The thinner the high-temperature layers and the farther apart, the more pronounced is the temperature variation of the average magnetization. This temperature dependence also can be investigated experimentally and used for a verification of our theory.

The spin dynamics are based on the generalized Bloch equation. Two different interactions contribute to the effective field H_{eff}, appearing therein: (i) The long-range dipolar interaction which is dominant in the low energy region of the magnon spectrum; (ii) the short-range exchange interaction which is important in the high energy part of the spectrum. In the pure dipolar limit we recovered the Damon-Eshbach modes, which have been studied previously only in single films or in superlattices consisting of alternating ferromagnetic and nonmagnetic materials. These modes are localized at the interfaces between the layers and their spectrum is strongly anisotropic for $\mathbf{k} \to 0$. This low energy part of the spectrum can be studied in light scattering experiments.

In the pure exchange limit the spin dynamics equation for a circular component m_+ reduces to an equation similar to the Schrödinger equation in a periodic potential with position dependent mass. The spectrum has the expected band structure, but the gaps disappear for certain values of wave vectors. This vanishing of gaps follows from the structure of the equation of motion, where the component of magnon wave number parallel to the layers $k_\parallel$ appears as a parameter which "tunes" the potential energy. In this sense this effect is similar to the term crossing in diatomic molecules. In two cases we also calculated the points in $(\mathbf{k},\omega)$ space where gaps vanish, namely (i) when $M_0(x)$ can be approximated by a step function. This approximation is relevant for thick layers in the low temperature region; (ii) for the "δ model," which describes the case of thin high-temperature layers submerged into low-temperature material.

If $k_\parallel \neq 0$, two kinds of energy bands in the magnon spectrum are clearly seen: narrow bands in the low-energy region and wide bands in the high energy one. This band structure can be understood solely from the knowledge of the bulk magnon dispersion relations of the layer constituents as follows. The "potential energy" in the equation describing propagation of magnons is approximately $k_\parallel^2 M_0(x)$. Hence, the low-energy magnons can freely propagate only in the layers with lower magnetization. The spectrum of these magnons can be calculated in some kind of tight-binding model, well known from the electron theory. This leads to the narrow band structure. On the other hand, the magnons with higher energies can freely propagate in both layers. This accounts for the wide bands.

The spectrum in the general case, where both dipolar and exchange interactions are included, has been studied numerically. The comparison of this spectrum with the dispersion relations in the two limiting cases of pure dipolar and pure exchange interactions shows the following: (i) if the parallel component of $\mathbf{k}$ is along the static magnetization $\mathbf{M}_0(x)$, the spectrum is qualitatively similar to the pure exchange case; (ii) for arbitrary directions of $\mathbf{k}$, in general, the previously degenerate levels split.

The calculated inelastic neutron scattering cross section shows that the vanishing of gaps leads to peaks in the intensity of scattered neutrons at special wave vectors and energies. We think that from an experimental point of view two predictions of our theory are of special interest: the above-mentioned increase of the cross section for $\mathbf{k}$ and ω in the vicinity of their gap-vanishing values, and the appearance of narrow magnon bands, because in this $(\mathbf{k},\omega)$ region the cross section shows clear band structure.

To conclude, we want to mention some further points of interest, which can be studied within the framework of our theory: the influence of different interface interactions on the statics and dynamics in such systems; critical phenomena, e.g., the crossover from layer dominated to three-dimensional critical behavior; the extension of our theory to other systems, such as antiferromagnets or structural phase transitions; the study of random or quasiperiodic multilayers.

ACKNOWLEDGMENT

This work has been supported in part by the German Federal Minister for Research and Technology (BMFT) under Contract No. 03-SC1TUM-0 and the Deutsche Forschungsgemeinschaft.

APPENDIX A: SEPARATE LAYERS CONNECTED BY BOUNDARY CONDITIONS

In our description the Ginzburg-Landau parameters and the order parameter are defined throughout the whole sample. Boundary conditions between the magnetization of these layers result only if for mathematical convenience discontinuous GL parameters are used in model calculations. An alternative approach is to consid-

er the magnetization density $\mathbf{M}_i(\mathbf{x})$ in each layer i and to decompose the total free energy into a sum of individual independent layer terms $F_i^l(\mathbf{M}_i)$ and interface terms F_i^s,

$$F=\sum_i F_i^l[\mathbf{M}_i]+\sum_i F_i^s[\mathbf{M}_i,\mathbf{M}_{i+1}] . \tag{A1}$$

Here F_i^l is the free energy of ith layer of the usual form

$$F_i^l[\mathbf{M}_i(x)]=\tfrac{1}{2}\int_{v_i} d^3x \left[a_i\mathbf{M}_i^2+\tfrac{1}{2}b_i(\mathbf{M}^2)^2+c_i\frac{\partial\mathbf{M}_i}{\partial x_k}\frac{\partial\mathbf{M}_i}{\partial x_k} -\mathbf{H}_i^m\mathbf{M}_i-2\mathbf{H}\mathbf{M}_i\right] , \tag{A2}$$

where a_i, b_i, and c_i are GL parameters and $\mathbf{H}_i^m$ is the demagnetization field in ith layer. The GL coefficients are assumed to be constant or very smooth functions of $\mathbf{x}\epsilon V_i$ in every layer.

The interface energy between layers i and $i+1$ is described by F_i^s and has the form

$$F_i^s(\mathbf{M}_i,\mathbf{M}_{i+1})=\int_{S_i} ds_i f^s(\mathbf{M}_i,\mathbf{M}_{i+1}) . \tag{A3}$$

The form of the surface free-energy density depends on the interactions on the interface and in general can be written as

$$f^s(\mathbf{M}_i,\mathbf{M}_{i+1})=A_{lm}\mathbf{M}_l\mathbf{M}_m+K_{lm}(\mathbf{n}\mathbf{M}_l)(\mathbf{n}\mathbf{M}_m) , \tag{A4}$$

with $l,m=i,i+1$ and $\mathbf{n}$ the normal to the interface. The first term describes the exchange and the second the anisotropic interactions at the interface. The form of the tensors A_{lm} and K_{lm} can be deduced either from microscopic calculations or from comparison of the experimental results with the predictions of theoretical models with different forms of these tensors.

Minimizing (A1) with respect to $\mathbf{M}_i(x)$ one obtains from the first term the GL equations

$$\frac{\delta F_i^l}{\delta\mathbf{M}_i(x)}=0 , \tag{A5}$$

which together with Maxwell's equations for $\mathbf{H}_i^m$ defines the "equations of motion" in ith layer. The minimization of the second term together with the electromagnetic boundary conditions provides the boundary conditions for this system of equations. It is worth noting that no assumptions about the continuity of $\mathbf{M}(\mathbf{x})$ (or its derivatives) at the interfaces are made. The order parameter can be continuous or discontinuous at the interfaces, depending on the form of $f^s(\mathbf{M}_i,\mathbf{M}_{i+1})$.

APPENDIX B: ULTRATHIN LAYERS

We consider here the so-called "δ model" used previously in the study of structural phase transitions with defects.[17] In this model one uses the GL functional (2.1) with GL coefficient $a(x)$ of the form

$$a(x)=a(T)+u_0\sum_n \delta[x-(n+\tfrac{1}{2})D] , \tag{B1}$$

where u_0 describes the strength of "defects." One also assumes that $a(T)=a'(T-T_c^0)$, where T_c^0 is the bare transition temperature of the medium. The GL coefficients b and c are usually taken to be constant. In our context this model represents very thin layers of material 2 with a very high transition temperature submerged into material 1.

Substituting (B1) into Eq. (2.4), with $\mathbf{H}=\mathbf{H}^m=0$, one gets

$$\left[a(T)+u_0\sum_n \delta[(n+\tfrac{1}{2})D-x]+b\mathbf{M}_0^2-c\Delta\right]\mathbf{M}_0(\mathbf{x})=0 . \tag{B2}$$

Hence the magnetization $\mathbf{M}_0(\mathbf{x})$ is continuous. Integrating Eq. (B2) around $x=(n+\frac{1}{2})D$, we obtain the condition on $\partial_x\mathbf{M}_0$

$$c(\partial_x\mathbf{M}_0[(n+\tfrac{1}{2})D^+]-\partial_x\mathbf{M}_0[(n+\tfrac{1}{2})D^-]) =u_0\mathbf{M}_0[(n+\tfrac{1}{2})D] . \tag{B3}$$

Here $\partial_x\mathbf{M}_0[(n+\frac{1}{2})D^+]$ and $\partial_x\mathbf{M}_0[(n+\frac{1}{2})D^-]$ denote the derivatives of $\mathbf{M}_0$ just right and left to the "defect" localized at $x=(n+\frac{1}{2})D$.

The transition temperature in this model can be obtained from expression (3.2), where the following substitutions have to be made: $D_1=D$, $D_2=0$, $c_1=c$, and $a_s=u_0/2$. Then we get for the transition temperature T_c the following implicit equation:

$$\tanh\left[\frac{D}{2\xi(T_c)}\right]=-\frac{V_0}{2} , \tag{B4}$$

where $\xi=\sqrt{c/|a(T)|}$ and $V_0=u_0(c|a(T)|)^{-1/2}$.

If the "defects" are far apart, i.e., $D\gg\xi(T_c)$, then Eq. (B4) can be solved readily and

$$T_c\simeq T_c^0+\frac{u_0^2}{4a'c} . \tag{B5}$$

This result has been previously obtained by Schmidt and Schwabl,[19] and we refer the reader to this reference for an extensive discussion of order parameter profiles in the "δ model."

Now we consider the spin dynamics in this model, defined by Eq. (4.19). Again we will be interested in the temperature region $T\ll T_c^0$ and consider only the low-lying spin wave modes with small wave vectors $k\ll\xi^{-1}$.

In this temperature region the magnetization profile is shown in Fig. 15. It is worth noting that the static magnetization $M_0(x)$ is strongly inhomogeneous and cannot be approximated by a step function, as has been done in Sec. IV.

To proceed further we introduce a new function

$$f(x)=m_+(x)/M_0(x) ,$$

which obeys the equation

$$-c\partial_x[M_0^2\partial_x f(x)]+\left[ck_\parallel^2M_0^2(x)-\frac{\omega}{\gamma}M_0(x)\right]f(x)=0 . \tag{B6}$$

Equation (B6) also implies that $f(x)$ and $\partial_x f(x)$ are continuous. Because of the symmetry of the "Hamiltoni-

an," the two linear independent one-cell solutions of Eq. (B6) can be chosen to be real functions with definite parity. Hence, we look for $f(x)$ in the form

$$f(x)=b(x)e^{iS(x)} , \tag{B7a}$$

where the real functions $b(x)$ and $S(x)$ are even and odd, respectively. The real (imaginary) part of $f(x)$ defines the one-cell solutions $u(\omega,x)$ ($g(\omega,x)$) considered in Sec. IV.

Substituting expression (B7a) into Eq. (B6) and separating real and imaginary parts in this equation, we see that $S(x)$ obeys the equation

$$M_0 b(x)\partial_x^2 S(x)+2\partial_x S(x)\partial_x(M_0 b(x))=0 . \tag{B7b}$$

The first integral of this equation reads

$$\partial_x S(x)=\frac{A}{cM_0^2(x)b^2(x)} , \tag{B7c}$$

where A is a constant of integration. Of course, the dispersion relation and all other physical quantities are independent of the choice of this constant. Substituting Eq. (B7c) into the real part of Eq. (B6), we obtain the equation for $b(x)$

$$c\partial_x(M_0^2(x)\partial_x b(x))=\frac{A^2}{cM_0^2(x)b^3(x)}+\left[k_\parallel^2 cM_0^2(x)-\frac{\omega}{\gamma}M_0(x)\right]b(x) . \tag{B7d}$$

In order to solve this nonlinear equation it is worth noting that for $\omega=k_\parallel=0$ the solution of Eq. (B6) is trivial, namely $f(x)=$const. Hence, for small ω and $k_\parallel$, it is plausible to look for $b(x)$ in the form

$$b(x)=1+a(x) , \tag{B7e}$$

where $a(x)\ll 1$. Now, Eqs. (B7c) and (B7d) can be solved perturbatively with respect to $a(x)$. Keeping only the leading terms in these equations, we obtain

$$c\partial_x(M_0^2(x)\partial_x a(x))=\frac{A^2}{cM_0^2(x)}+k_\parallel^2 cM_0^2(x)-\frac{\omega}{\gamma}M_0(x) , \tag{B8a}$$

$$S'(x)=\frac{A}{cM_0^2(x)} . \tag{B8b}$$

Integrating Eq. (B8a), we obtain

$$a(x)=\int_0^x\frac{dx'}{cM_0^2(x')}\int_0^{x'}dx''\left[\frac{A^2}{cM_0^2(x'')}+k_\parallel^2 cM_0^2(x'')-\frac{\omega}{\gamma}M_0(x'')\right] . \tag{B9}$$

In order to estimate the value of $a(D/2)$, we consider now the realistic case $D\gg\xi$. Then, as can be seen from Fig. 15, the magnetization $M_0(x)$ reaches its bulk value M_{0b} for $x\ll(D/2-\xi)$, but changes rapidly in a region

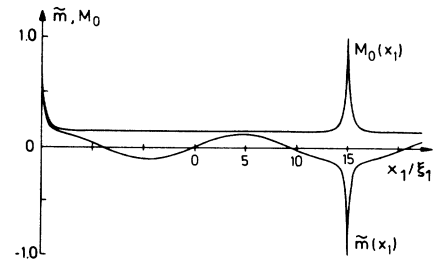

FIG. 15. The magnetization $M_0(x)$ and the real part of the magnon wave function $\tilde{m}(x)=\mathrm{Re}m_+(x)$ for ultrathin layers at low temperatures: $\xi_1/\xi_2=10$, $D/\xi_1=30$, $k_\parallel=0.32/\xi_1$; $k_\perp=3\pi/D$.

of order ξ around the "defects." Substituting into (B9) the approximate form for $M_0(x)$

$$M_0(x)\simeq\begin{cases}M_{0b} & \text{for } x\le(D/2-\xi) ,\\ M_0(x) & \text{for } D/2-\xi\le x\le D/2 ,\end{cases} \tag{B10}$$

and integrating this expression, one sees that

$$a\left[\frac{D}{2}\right]\simeq\left[\frac{A^2}{c^2M_{0b}^4}+k_\parallel^2-\frac{\omega}{\gamma cM_{0b}}\right]\frac{D^2}{2}+0(k^2\xi^2) . \tag{B11}$$

We now use the freedom in the choice of the constant of integration A. To justify the previously made assumption $a\ll 1$, we choose

$$A^2=cM_{0b}^3\left[\frac{\omega}{\gamma}-cM_{0b}k_\parallel^2\right] . \tag{B12}$$

Then the expression in the brackets of Eq. (B11) vanishes and $a(x)$ is of order $(k^2\xi^2)\ll 1$, no matter how large the period D is. Now integrating Eq. (B8b), we can find $S(x)$.

Having defined $a(x)$ and $S(x)$, we can now calculate the band structure as well as the gap vanishing conditions in this model. The odd and even one-cell solutions $u(\omega,x)$ and $g(\omega,x)$ of Eq. (B6) (see also Sec. IV) are

$$\begin{aligned}u(\omega,x)&=(1+a(x))\sin[S(x)] \quad \text{for } x\le\left|\frac{D}{2}\right| ,\\ g(\omega,x)&=(1+a(x))\cos[S(x)] \quad \text{for } x\le\left|\frac{D}{2}\right| .\end{aligned} \tag{B13}$$

Substituting $a(x)$ and $S(x)$ defined by (B8) and (B12) into the conditions for a vanishing gap, namely that $u(\omega,d/2)=\partial_x g(\omega,D/2)=0$ or $g(\omega,D/2)=\partial_x u(\omega,D/2)=0$, we obtain that the gaps vanish for the following values of $k_\parallel$:

$$(k_\parallel)_n=\frac{\pi n}{(D-\Delta)}\left[\frac{B_2}{B_1-B_2}\right]^{1/2} . \tag{B14}$$

Here n is a positive integer and Δ, B_1, and B_2 are

$$\Delta=\int_{-D/2}^{D/2}\left[1-\frac{M_{0b}^2}{M_0^2(x)}\right]dx\ , \tag{B15a}$$

$$B_1-\int_{-D/2}^{D/2}\frac{M_0^2(x)}{M_{0b}^2}\left[1-\frac{M_{0b}^4}{M_0^4(x)}\right]dx\ , \tag{B15b}$$

$$B_2=\int_{-D/2}^{D/2}\frac{M_0(x)}{M_{0b}}\left[1-\frac{M_{0b}^3}{M_0^3(x)}\right]dx\ . \tag{B15c}$$

The frequencies ω_n where the gaps vanish can be also calculated

$$\omega_n=\frac{\gamma c M_{0b}B_1\pi^2n^2}{(B_1-B_2)(D-\Delta)^2}\ . \tag{B16}$$

It is worth mentioning that if we define $p_0=k_\parallel(B_1/B_2-1)^{1/2}$, then expression (B14) can be written as

$$p_0(D-\Delta)=\pi n\ . \tag{B17}$$

This is very similar to condition (4.22b) with $D_2=0$ and a new effective thickness $D_1=D-\Delta$.

In Fig. 15 we also plot the real part of the magnon wave function $\bar{m}(x)=\mathrm{Re}m_+(x)$. It is seen that the wave function is enhanced in proportion to the magnetization.

APPENDIX C: COMPUTATION OF THE DISPERSION RELATION

The system of Eqs. (4.4), considered as a system of first-order differential equations for m_x, m_y, $\varphi(x)$, and their derivatives, has six independent solutions, which we denote by $\mathbf{V}^j(x)$, with $j=\pm1,\pm2,\pm3$. If one takes for the static magnetization $M_0(x)$ the "step-form" [Eq. (4.9)], Eqs. (4.4) can be solved readily in each layer and $\mathbf{V}^j(x)$ has the form

$$\mathbf{V}_\alpha^j=\begin{bmatrix}\lambda_\alpha^j(x)\\ \partial_x\lambda_\alpha^j(x)\end{bmatrix}\ , \tag{C1}$$

with $\alpha=1,2$ referring to layers 1 and 2. The vectors $\lambda_\alpha^j(x)$ read

$$\lambda_\alpha^{\pm1}=e^{\pm iq_\alpha x}\begin{bmatrix}\mp4\pi M_{b\alpha}q_\alpha k_y+\frac{i\omega}{\gamma}(k_\parallel^2+q_\alpha^2)\\ \frac{\omega^2}{\gamma^2c_\alpha M_{b\alpha}}-4\pi M_{b\alpha}k_y^2\\ -4\pi i\left[\pm\frac{i\omega}{\gamma}q_\alpha+k_yc_\alpha M_{b\alpha}(k_\parallel^2+q_\alpha^2)\right]\end{bmatrix},\quad \lambda_\alpha^{\pm2}=e^{\mp\kappa_\alpha x}\begin{bmatrix}\mp4\pi iM_{b\alpha}\kappa_\alpha k_y-\frac{i\omega}{\gamma}(\kappa_\alpha^2-k_\parallel^2)\\ \frac{\omega^2}{\gamma^2c_\alpha M_{b\alpha}}-4\pi M_{b\alpha}k_y^2\\ -4\pi i\left[\mp\frac{\omega}{\gamma}\kappa_\alpha+k_yc_\alpha M_{b\alpha}(k_\parallel^2-\kappa_\alpha^2)\right]\end{bmatrix},$$

$$\lambda_\alpha^{\pm3}=e^{\mp k_\parallel x}\begin{bmatrix}\pm ik_y\\ k_\parallel\\ \mp\frac{i\omega}{\gamma M_{b\alpha}}\end{bmatrix}. \tag{C2}$$

Here $M_{b\alpha}$ is the bulk magnetization in layer α and q_α, κ_α are given by

$$q_\alpha=\left\{-k_\parallel^2-\frac{2\pi}{c_\alpha}+\left[\left[\frac{2\pi}{c_\alpha}\right]^2+\left[\frac{\omega}{c_\alpha M_{b\alpha}\gamma}\right]^2+\frac{4\pi k_z^2}{c_\alpha}\right]^{1/2}\right\}^{1/2},$$

$$\kappa_\alpha=\left\{k_\parallel^2+\frac{2\pi}{c_\alpha}+\left[\left[\frac{2\pi}{c_\alpha}\right]^2+\left[\frac{\omega}{c_\alpha M_{b\alpha}\gamma}\right]^2+\frac{4\pi k_z^2}{c_\alpha}\right]^{1/2}\right\}^{1/2}. \tag{C3}$$

The general one-cell solutions of Eqs. (4.4) can now be written as

$$\mathbf{f}(\mathbf{x})=\sum_{\alpha=1,2}\Theta\left[\tfrac{1}{2}D_\alpha-\left|x-\left[\frac{\alpha-1}{2}\right]D\right|\right]\sum_j A_\alpha^j\mathbf{V}_\alpha^j(x)\ , \tag{C4}$$

where A_α^j are 12 unknown coefficients.

At the interfaces these solutions must satisfy the boundary conditions for $\mathbf{m}$ and $\partial_x\mathbf{m}$, as discussed in Sec. IV, as well as the conditions on $\varphi(x)$ following from Maxwell's equations, namely the continuity of $\varphi(x)$ and $\partial_x\varphi-4\pi m_x(x)$. Together with the Bloch condition $\mathbf{f}(x+D)=\mathbf{f}(x)\exp(ikD)$, this gives rise to 12 linear algebraic equations for the unknown coefficients A_α^j. For nonzero solutions of this algebraic system, the determinant must vanish, which defines the dispersion relation.

[1]Ch. Sauer and W. Zinn, Kernforschungsanlage Jülich GmbH, Jahresbericht 85/86 (1986).
[2]J. P. Castera, J. Appl. Phys. **55**, 2506 (1984).
[3]C. F. Majkrzak, J. D. Axe, and P. Böni, J. Appl. Phys. **57**, 3657 (1985).
[4]F. Mezei and P. A. Dagleish, Commun. Phys. **2**, 41 (1977).
[5]R. E. Camley, T. S. Rahman, and D. L. Mills, Phys. Rev. B **27**, 261 (1983).
[6]P. Gruenberg and K. Mika, Phys. Rev. B **27**, 2955 (1983).
[7]L. L. Hinchey and D. L. Mills, Phys. Rev. B **33**, 3329 (1986).
[8]F. Herman and P. Lambin, J. Appl. Phys. **57**, 3654 (1985).
[9]H. K. Wong, H. Q. Yang, J. E. Hilliard, and J. B. Ketterson, J. Appl. Phys. **57**, 3660 (1985).
[10]L. Dobrzynski, B. Djafari-Rouhani, and H. Puszkarski, Phys. Rev. B **33**, 3251 (1986).
[11]E. L. Albuquerque, P. Fulco, and D. R. Tilley, Solid State Commun. **58**, 41 (1986).
[12]R. P. van Stapele, F. J. A. M. Greidanus, and J. W. Smits, J. Appl. Phys. **57**, 1282 (1985).
[13]F. Fishman, F. Schwabl, and D. Schwenk, Phys. Lett. A **121**, 192 (1987).
[14]S. Ma, and G. F. Mazenko, Phys. Rev. B **11**, 4077 (1975).
[15]R. W. Damon and J. R. Eshbach, J. Phys. Chem. Solids **19**, 308 (1961).
[16]H. Suhl, Appl. Phys. **8**, 217 (1975).
[17]H. Schmidt and F. Schwabl, Phys. Lett. **61A**, 476 (1977).
[18]A. J. Akhiezer, V. G. Bar'yakthar, and S. V. Peletminskii, *Spin Waves* (North-Holland, Amsterdam, 1968).
[19]H. Schmidt and F. Schwabl, Z. Phys. B **30**, 197 (1978).
[20]L. Passel, O. W. Dietrich, and J. Als-Nielsen, Phys. Rev. B **14**, 4897 (1976); **14**, 4908 (1976); **14**, 4923 (1976).
[21]D. Schwenk, doctoral thesis, Technische Universitël München, 1988, unpublished.
[22]P. F. Byrd and M. D. Frieman, *Handbook of Elliptic Integrals for Engineers and Scientists,* (Springer, New York, 1971).
[23]M. G. Cottam and D. J. Lockwood, *Lightscattering in Magnetic Solids* (Wiley, New York, 1986).
[24]L. D. Landau and E. M. Lifshitz, *Course of Theoretical Physics,* Vol. 5 of *Statistical Physics* (Pergamon, London, 1959).
[25]P. Gruenberg and F. Metawe, Phys. Rev. Lett. **39**, 1561 (1977).
[26]H. M. James, Phys. Rev. **76**, 1602 (1949).
[27]H. Jones, *The Theory of Brillouin Zones and Electronic States in Crystals* (North-Holland, Amsterdam, 1975).
[28]L. D. Landau and E. M. Lifshitz, *Course of Theoretical Physics,* Vol. 3 of *Quantum Mechanics* (Pergamon, Oxford, 1958).
[29]K. Vayhinger and H. Kronmüller, J. Magn. Magn. Mater. **62**, 159 (1986).
[30]E. Kamke, *Differentialgleichungen, Lösungsmethoden und Lösungen I.* (Akademische Verlagsgesellschaft, Geest & Portig, Leipzig, 1956).
[31]Marshall and Lovesy, *Theory of Thermal Neutron Scattering* (Oxford Press, Oxford, 1971).
[32]For the numerical calculation it is easier to use instead of Eq. (5.14) the equivalent form for the response function

$$G_+(x,x',q_\parallel,\omega)=(\Theta(x-x')m_1(x)m_2(x') + \Theta(x'-x)m_1(x')m_2(x))/W(m_1,m_2)\ ,$$

where m_1 and m_2 are two linear independent solutions of Eq. (5.12a) [with substitution $\varepsilon_n(\mathbf{k})\rightarrow\omega$], and $W(m_1,m_2)$ is the Wronskinian (See Ref. 30).